WATER RESOURCES RESEARCH, VOL. 49, 488–506, doi:10.1029/2012WR012380, 2013

Solutions for the diurnally forced advection-diffusion equation to estimate bulk fluid velocity and diffusivity in streambeds from temperature time series

Charles H. Luce,[1] Daniele Tonina,[2] Frank Gariglio,[2] and Ralph Applebee[3]

Received 15 May 2012; revised 16 November 2012; accepted 21 November 2012; published 29 January 2013.

[1] Work over the last decade has documented methods for estimating fluxes between streams and streambeds from time series of temperature at two depths in the streambed. We present substantial extension to the existing theory and practice of using temperature time series to estimate streambed water fluxes and thermal properties, including (1) a new explicit analytical solution to predict one-dimensional fluid velocity from amplitude and phase information; (2) an inverse function, also with explicit formulation; (3) methods to estimate fluid velocity from temperature measurements with unknown depths; (4) methods to estimate thermal diffusivity from the temperature time series when measurement depths are known; (5) methods to track streambed elevation between two sensors, given knowledge of the thermal diffusivity from (4) above; (6) methods to directly calculate the potential error in velocity estimates based on the measurement error characteristics; and (7) methods for validation of parameter estimates. We also provide discussion and theoretical insights developed from the solutions to better understand the physics and scaling of the propagation of the diurnal temperature variation through the streambed. In particular, we note that the equations developed do not replace existing equations applied to the analysis, rather they are new equations representing new aspects of the process, and, as a consequence, they increase the amount of information that can be derived from a particular set of thermal measurements.

Citation: Luce, C. H., D. Tonina, F. Gariglio, and R. Applebee (2013), Solutions for the diurnally forced advection-diffusion equation to estimate bulk fluid velocity and diffusivity in streambeds from temperature time series, *Water Resour. Res.*, *49*, doi:10.1029/2012WR012380.

1. Introduction

[2] The flow of water in the streambed is important to aquatic organisms that use the streambed for part or all of their life cycle [*Baxter and Hauer*, 2000; *Edwards*, 1998; *Orghidan*, 1959; *Stanford*, 2006; *Stanford and Ward*, 1988; *Tonina and Buffington*, 2009a, 2009b; *Wondzell*, 2011], potentially for buffering stream temperatures [*Arrigoni et al*., 2008; *Moore et al*., 2005; *Tonina and Buffington*, 2009a] and for transport of both conservative [*Elliott and Brooks*, 1997; *Marzadri et al*., 2010; *Salehin et al*., 2004; *Savant et al*., 1987; *Tonina and Buffington*, 2007, 2011] and reactive [*Boano et al*., 2010; *Marzadri et al*., 2011, 2012; *Triska et al*., 1993] solutes and suspended particles [*Ren and Packman*, 2004, 2007]. Seepage of water from stream channels is an important component of groundwater recharge as well [*Constantz*, 2008; *Constantz and Thomas*, 1996; *Constantz and Stonestorm*, 2003]. In ecological contexts, flows of low velocity and the differences between upwelling and downwelling flows can be important [*Edwards*, 1998; *Stanford and Ward*, 1988, 1993; *Tonina and Buffington*, 2009b]. Temporal variations in hyporheic flows are important in ecological, water resource, and water quality contexts and have particularly been noted at seasonal time scales [*Schmidt et al*., 2011; *Shope et al*., 2012; *Wroblicky et al*., 1998].

[3] Measuring flow can be difficult, and a number of methods are used to estimate the magnitude and/or direction of hyporheic flow, including pressure gradient measurements [*Anderson et al*., 2005; *Baxter and Hauer*, 2000; *Geist*, 2000; *Kasahara and Hill*, 2006; *Lee and Cherry*, 1978; *Terhune*, 1958; *Tonina and Buffington*, 2007; *Valett et al*., 1994], temperature measurements [*Hatch et al*., 2006; *Keery et al*., 2007], and other tracer techniques [*Clayton et al*., 1996; *Tonina and Buffington*, 2009a; *Zarnetske et al*., 2008]. Use of temperature data loggers to compare diurnal fluctuations of water temperature at different depths in the streambed has substantial benefits for monitoring streambed water fluxes over time compared with other methods in terms of the amount and quality of information obtained and ease of use and expense [*Constantz*, 2008; *Hatch et al*., 2006; *Lautz*, 2012; *Shanafield et al*., 2011; *Stallman*, 1965].

[1]Department of Agriculture, Rocky Mountain Research Station, U.S. Forest Service, Boise, Idaho, USA.
[2]Center for Ecohydraulics Research, College of Engineering, University of Idaho, Boise, Idaho, USA.
[3]Professor Emeritus, College of Idaho, Caldwell, Idaho, USA.

Corresponding author: C. H. Luce, Department of Agriculture, Rocky Mountain Research Station, U.S. Forest Service, 322 E Front St., Ste. 401, Boise, ID 83702, USA. (cluce@fs.fed.us)

©2012. American Geophysical Union. All Rights Reserved.
0043-1397/13/2012WR012380

[4] Thermal tracer data are commonly analyzed based on the relative amplitude of temperature cycles, A, at two depths, specifically, the log of the ratio of the diurnal temperature variations at each depth, $\ln(A_2/A_1)$, with the subscripts 1 and 2 indicating the shallow and deep depths, z_1 and z_2, respectively, or based on the phase differences in the temperature cycles at those depths ($\phi_2 - \phi_1$; Figure 1). Substantial work has been completed on the sensitivity of these two related analytical techniques to parameters, errors in parameters, or violation of model assumptions [*Goto et al*., 2005; *Hatch et al*., 2006; *Lautz*, 2010; *Shanafield et al*., 2011]. Much less work has been done with solutions using the ratio of the log-amplitude ratio to the phase difference, which we call η,

$$\eta = \frac{-\ln(A_2/A_1)}{\phi_2 - \phi_1}, \tag{1}$$

since it was briefly introduced by *Stallman* [1965]. In this paper, we further develop the approach, providing explicit analytical solutions for the thermal Peclet number when only η is known and for thermal diffusivity and the advective component of thermal velocity when η is calculated from data at known depths. We also demonstrate the additional utility that can be realized for validating data or monitoring streambed scour over time. Finally, we apply the equations to show error properties relative to measurements.

2. Theory

2.1. Review

[5] Vertical heat fluxes through a stream bottom are generally considered as a combination of conduction and convection. The governing partial differential equation (PDE) is derived from conservation of energy, where the change in storage of heat can be broken down into the divergences of the conductive and advective fluxes.

$$\rho_m c_m \frac{\partial T}{\partial t} = \lambda_m \frac{\partial^2 T}{\partial z^2} - q\rho_w c_w \frac{\partial T}{\partial z}, \tag{2}$$

where the subscript m denotes the sediment-water system, and w indicates the water, which is the moving portion of the system [*Stallman*, 1965]. Further, T is the temperature (°C); t is the time (s); z is the depth into the streambed (m), positive downward; q is the Darcian fluid velocity or seepage flux (m s^{-1}; positive flux is downward); ρ is the density of the specified medium (water or matrix; kg m^{-3}); c is the specific heat of specified medium (water or matrix; J kg^{-1} °C^{-1}); and λ_m is the thermal conductivity of the sediment-water matrix (W m^{-1} °C^{-1}).

[6] This can be rearranged into the one-dimensional advection-diffusion equation:

$$\frac{\partial T}{\partial t} = \kappa_e \frac{\partial^2 T}{\partial z^2} - v_t \frac{\partial T}{\partial z} \tag{3}$$

[*Suzuki*, 1960], which summarizes all of the constants in equation (2) into two parameters: one related to heat transport via diffusion and the other to heat transport by movement of the fluid. These two parameters are related to the previously listed constants.

[7] κ_e is the effective thermal diffusivity (m^2 s^{-1}):

$$\kappa_e = \frac{\lambda m}{\rho_m c_m}. \tag{4}$$

Although the effects of dispersivity caused by microeddies in the fluid as it moves through pores is commonly included with the effective thermal diffusivity [*Hatch et al*., 2006; *Keery et al*., 2007], we neglect it because there are issues of identifiability between the effects of dispersion and diffusion [*Anderson*, 2005].

[8] v_t is the areally averaged rate of heat movement induced by movement of water through the bed (m s^{-1}; positive flux is downward); v_t is related to the areally averaged water velocity as expressed in the following equation:

$$v_t = q \frac{\rho_w c_w}{\rho_m c_m}. \tag{5}$$

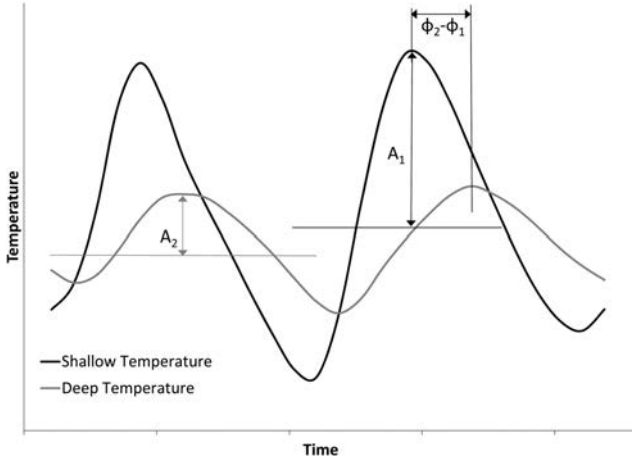

Figure 1. Definition sketch for amplitude ratio (A_2/A_1) and $\Delta_\phi = \phi_2 - \phi_1$ (note equations in text take $\Delta\phi$ in radians) drawn on observed time series from *Gariglio* [2012]. In general applications, the phase and amplitude of each time series is found separately. Note that this figure also shows common violations of the boundary conditions (6): the mean temperature at depth is not the same as that at the surface, and the series are slightly asymmetric and not perfectly sinusoidal. These can affect the accuracy of the solutions [*Lautz*, 2010; *Shanafield et al*., 2011].

[9] Although v_t is sometimes referred to as the "thermal front velocity," the terminology can be confusing, as the term is actually separate from, and independent of, conductive thermal fluxes. Because we later derive phase velocities for the diurnal temperature wave, including both the diffusive and advective components, that look much more like "front velocities," we have instead adopted the phrase "advective thermal velocity" for v_t.

[10] During some months of the year, when streams are not ice covered for instance, the boundary condition of

interest is a diurnally varying temperature in the stream water with daily average temperature, T_μ, at the top

$$T(0,t) = T_\mu + A\cos(\omega t) \tag{6a}$$

and a semi-infinite domain with

$$\lim_{z\to\infty} T(z,t) = T_\mu, \tag{6b}$$

where A is the magnitude of diurnal temperature amplitude at the surface (°C), ω is the angular frequency for diurnal frequency (s^{-1}), or

$$\omega = \frac{2\pi}{P}, \tag{7}$$

where P is the period of the oscillation (s), 1 day in the case of diurnal variations.

[11] The PDE (3) has a solution

$$T(z,t) = T_\mu + Ae^{-az}\cos(\omega t - bz) \tag{8}$$

with

$$a = \frac{1}{2\kappa_e}\left(\sqrt{\frac{\sqrt{v_t^4 + (4\omega\kappa_e)^2} + v_t^2}{2}} - v_t\right) \tag{9}$$

and

$$b = \frac{1}{2\kappa_e}\sqrt{\frac{\sqrt{v_t^4 + (4\omega\kappa_e)^2} - v_t^2}{2}} \tag{10}$$

[*Goto et al*., 2005; *Hatch et al*., 2006; *Keery et al*., 2007; *Stallman*, 1965]. These two parameters can be estimated from two time series of temperature measurements taken at two depths, here denoted with 1 for the shallower sensor, at depth z_1, and 2 for the more deeply buried sensor, at depth z_2 (see Figure 1 for definition sketch). The term a may be approximated by the ratio of the daily temperature ranges (amplitude) measured the two depths divided by the vertical distance between the sensors:

$$a \approx \frac{-\ln\left(\frac{A_2}{A_1}\right)}{(z_2 - z_1)} = \frac{-\ln\left(\frac{A_2}{A_1}\right)}{\Delta z}. \tag{11}$$

The parameter b can be estimated from the difference in the timing of the diurnal oscillation at each depth, given as the difference in the phase, ϕ (here in angular units, e.g., radians), of the diurnal temperature wave at each depth, again divided by the vertical distance between sensors 1 and 2.

$$b \approx \frac{\phi_2 - \phi_1}{z_2 - z_1} = \frac{\phi_2 - \phi_1}{\Delta z}. \tag{12}$$

Fluid velocity has commonly been estimated based on equations (9)–(12) using a priori estimates of the bulk thermal diffusivity [e.g., *Hatch et al*., 2006].

[12] For a given sinusoidal time series, the amplitude ratio and phase difference can be found through a range of techniques. One can just look over a given 24 h period and compare temperature ranges and the difference in timing of peaks, noting that ϕ is in angular units with 2π radians in a 24 h period. Isolating a period of several days with a relatively consistent pattern, one can apply a Fourier transform to the data and isolate the effective amplitude and phase for each sinusoidal time series [e.g., *Luce and Tarboton*, 2010]. One can also apply tools like dynamic harmonic regression using the Captain Toolbox [*Taylor et al*., 2007] to obtain phase and amplitude estimates for diurnal patterns in the temperature time series on a continuous time basis.

2.2. Derivation of Nondimensional Form

[13] Under strictly diffusive conditions, specifically when $v_t = 0$, we can define two useful variables that relate to the diffusivity of the medium: z_d and v_d. The variable z_d is the diurnal damping depth, the depth at which the amplitude of daily temperature oscillations is $1/e$ of that at the surface [e.g., *Carslaw and Jaeger*, 1959; *Luce and Tarboton*, 2010; *Stallman*, 1965]:

$$z_d = \sqrt{\frac{2\kappa_e}{\omega}}. \tag{13}$$

The phase velocity of the diffusive temperature wave into the streambed is as follows:

$$v_d = \sqrt{2\omega\kappa_e}. \tag{14}$$

[14] We can nondimensionalize the PDE (3) and boundary condition (6) using the following dimensionless variables:

$$U = \frac{T - T_\mu}{A}, \tag{15a}$$

$$\tau = \omega t, \tag{15b}$$

$$x = \frac{z}{z_d} = \frac{z}{\sqrt{\frac{2\kappa_e}{\omega}}}, \tag{15c}$$

[15] Differentiating, we obtain

$$\partial T = A\partial U, \tag{16a}$$

$$\partial t = \frac{\partial\tau}{\omega}, \tag{16b}$$

$$\partial z = \sqrt{\frac{2\kappa_e}{\omega}}\,\partial x, \tag{16c}$$

which can be substituted directly into (3), yielding

$$\frac{\omega A\partial U}{\partial \tau} = \kappa_e \frac{A\partial^2 U}{(2\kappa_e/\omega)\partial x^2} - v_t \frac{A\partial U}{\sqrt{2\kappa_e/\omega}\,\partial x}, \tag{17}$$

which simplifies to

$$\frac{\partial U}{\partial \tau} = \frac{\partial^2 U}{\partial x^2} - v_t \frac{\partial U}{\sqrt{2\omega\kappa_e}\partial x} \tag{18}$$

or

$$\frac{\partial U}{\partial \tau} = \frac{1}{2}\frac{\partial^2 U}{\partial x^2} - \frac{v_t}{v_d}\frac{\partial U}{\partial x}. \tag{19}$$

[16] If we define a dimensionless advective thermal velocity

$$v_* = \frac{v_t}{v_d}, \tag{20}$$

then equation (19) further simplifies to

$$\frac{\partial U}{\partial \tau} = \frac{1}{2}\frac{\partial^2 U}{\partial x^2} - v_*\frac{\partial U}{\partial x}, \tag{21}$$

and the boundary conditions become

$$U(0,t) = \cos\tau, \tag{22a}$$

$$\lim_{x\to\infty} U(x,t) = 0, \tag{22b}$$

showing that the advection-diffusion equation with sinusoidal boundary conditions can be characterized with one parameter related to the ratio of the advective thermal velocity to the square root of thermal diffusivity.

[17] The relative contribution of the fluid velocity and diffusion to thermal transfer is given by the thermal Peclet number, *Pe* [*Anderson*, 2005]. It is readily identified as the ratio of the coefficients for the advective and diffusive terms in the PDE (21), $v_*/(1/2)$. In the case of the prescribed boundary conditions, the diffusive propagation of the daily temperature "wave" provides a characteristic velocity and time. This can be viewed as a particular Peclet number with the advective thermal velocity, v_t, as the scaling velocity and the thermal damping depth, z_d, as the scaling length. Alternatively, it may be viewed with $1/\omega$ as a scaling time:

$$Pe = 2v_* = 2\frac{v_t}{v_d} = \frac{2v_t}{\sqrt{2\omega\kappa_e}} = \frac{2v_t z_d}{\sqrt{2\omega\kappa_e}\sqrt{2\kappa_e/\omega}} = \frac{v_t z_d}{\kappa_e}. \tag{23}$$

2.3. Solutions to the Nondimensional Form

[18] The PDE (21) has solution in the form

$$U(\tau,x) = e^{-\alpha x}\cos(\tau - \beta x), \tag{24}$$

where α is the scaled amplitude damping rate (per unit scaled depth) parameter, and β is the scaled phase shift rate parameter. This solution automatically meets the first boundary condition (22a) regardless of parameters and satisfies the second boundary condition (22b) when $\alpha > 0$.

[19] U is the time series of temperature anomalies from the mean normalized by the daily temperature amplitude (centered and scaled temperature). The value of α can be estimated from a Fourier analysis of either the centered and scaled temperature time series (U) or the raw temperature time series (T) by looking at the ratio of the amplitudes at two different depths divided by the rescaled depths, similar to approaches described earlier:

$$\alpha \approx \frac{-\ln(A_2/A_1)}{x_2 - x_1} = \frac{-\ln(A_r)}{\Delta x}, \tag{25}$$

where A_2 and A_1 are the diurnal temperature amplitude at rescaled depths x_2 and x_1, respectively. Similarly, the phase rate parameters can be estimated from the change in phase of either U or T,

$$\beta \approx \frac{\phi_2 - \phi_1}{x_2 - x_1} = \frac{\Delta\phi}{\Delta x}. \tag{26}$$

For tracking differences between the dimensionless and original solutions, note that

$$\alpha x = az \quad \text{and} \quad \beta x = bz. \tag{27}$$

The remainder of this section discusses how to apply these parameter estimates to estimate the velocity and diffusivity parameters in the original PDEs (3) and (21).

[20] From the solution (24), we can write the following derivatives that are used in PDE (21):

$$\frac{\partial U}{\partial \tau} = -e^{-\alpha x}\sin(\tau - \beta x), \tag{28a}$$

$$\frac{\partial U}{\partial x} = -\alpha e^{-\alpha x}\cos(\tau - \beta x) + \beta e^{-\alpha x}\sin(\tau - \beta x), \tag{28b}$$

$$\frac{\partial^2 U}{\partial x^2} = (\alpha^2 - \beta^2)e^{-\alpha x}\cos(\tau - \beta x) - 2\alpha\beta e^{-\alpha x}\sin(\tau - \beta x). \tag{28c}$$

Substituting these into equation (21) yields

$$\begin{aligned} -e^{-\alpha x}\sin(\tau - \beta x) = \frac{1}{2}[&(\alpha^2 - \beta^2)e^{-\alpha x}\cos(\tau - \beta x) \\ &- 2\alpha\beta e^{-\alpha x}\sin(\tau - \beta x)] \\ &- v_*[-\alpha e^{-\alpha x}\cos(\tau - \beta x) + \beta e^{-\alpha x}\sin(\tau - \beta x)]. \end{aligned} \tag{29}$$

The factor, $e^{-\alpha x}$, is common to all terms, and we can group terms by their cosine or sine factor to give

$$\begin{aligned} &\frac{1}{2}(\alpha^2 - \beta^2 + 2\alpha v_*)\cos(\tau - \beta x) + (1 - \beta\alpha - \beta v_*) \\ &\quad \sin(\tau - \beta x) = 0. \end{aligned} \tag{30}$$

[21] Note that any linear combination of sine and cosine can be rewritten as a sine wave with a different amplitude and phase, e.g.,

$$C_1\cos(y) + C_2\sin(y) = C_3\sin(y + w), \tag{31}$$

where

$$C_3 = \sqrt{C_1^2 + C_2^2}. \tag{32}$$

If C_3 is zero, then C_1 and C_2 must also both be zero giving us the following two equations:

$$\alpha^2 - \beta^2 + 2\alpha v_* = 0 \tag{33}$$

and

$$1 - \beta(\alpha + v_*) = 0. \tag{34}$$

[22] These equations can be used to derive a number of useful relationships in the analysis of temperature-time-series data. Either can be used alone to estimate v_*, but there are other useful relationships that can be derived from equations (33) and (34). We illustrate four different solution strategies, isolating relationships among (1) v_* and α, (2) v_* and β, (3) v_* and the ratio of α to β, and (4) β and α, each providing unique information about the system. We begin with (1) and (2) because those are most familiar and follow with the (3) and (4) because they demonstrate a valuable extension of previously applied approaches.

2.3.1. Relationships Between Velocity and Either (1) Amplitude Damping or (2) Phase Shift

[23] Completing the square on equation (33),

$$\alpha^2 + 2\alpha v_* + v_*^2 - \beta^2 - v_*^2 = 0, \tag{35a}$$

$$(\alpha + v_*)^2 = \beta^2 + v_*^2. \tag{35b}$$

From equation (34),

$$\beta = \frac{1}{\alpha + v_*}, \tag{36}$$

which can be substituted into equation (35b):

$$(\alpha + v_*)^2 = \frac{1}{(\alpha + v_*)^2} + v_*^2. \tag{37}$$

Simplifying to show the full quartic equation:

$$(\alpha + v_*)^4 - v_*^2(\alpha + v_*)^2 - 1 = 0. \tag{38}$$

Completing the square by adding and subtracting $v_*^4/4$ and simplifying

$$[(\alpha + v_*)^2 - v_*^2/2]^2 = \frac{v_*^4}{4} + 1 \tag{39}$$

or

$$(\alpha + v_*)^2 - \frac{v_*^2}{2} = \frac{1}{2}\sqrt{v_*^4 + 4}. \tag{40}$$

Yielding

$$\alpha = \sqrt{\frac{\sqrt{v_*^4 + 4} + v_*^2}{2}} - v_*, \tag{41}$$

which relates amplitude damping between two sensors to the dimensionless velocity. When $v_* = 0$, $\alpha = 1$. Equation (41) is the dimensionless analog to equations (9) above and (4b) in *Hatch et al*. [2006].

[24] Continuing and substituting equations (41) into (36), by first moving the v_* term in equation (41) back to the left side,

$$\beta = \sqrt{\frac{2}{\sqrt{v_*^4 + 4} + v_*^2}}. \tag{42}$$

Noting that

$$\left(\sqrt{v_*^4 + 4} + v_*^2\right) \cdot \left(\sqrt{v_*^4 + 4} - v_*^2\right) = 4, \tag{43}$$

we obtain the following equation:

$$\beta = \sqrt{\frac{\sqrt{v_*^4 + 4} - v_*^2}{2}}, \tag{44}$$

which is analogous to equations (10) above and (5b) in *Hatch et al*. [2006]. Equation (44) also shows that β is constrained to the interval (0,1] and reaches its maximum at $v_* = 0$. The variable β asymptotically approaches 0, as v_* goes to large positive or negative values.

2.3.2. Relationships Between Velocity and the Ratio of Amplitude Damping to Phase Shift

[25] Obtaining estimates of either α or β from equation (25) or (26) requires knowledge of sensor depth and the diffusivity of the medium, and there are times when depth and diffusivity may not be known with precision a priori. In such a case, the ratio of the amplitude damping to the phase shift becomes useful, because the rescaled depth is eliminated. We define a new parameter, η,

$$\eta = \frac{\alpha}{\beta} = \frac{-\ln(A_r)}{\Delta\phi}. \tag{45}$$

When $v_* = 0$, diffusive conditions, η, α, and β, are all equal to 1. Based on earlier discussion, both α and β are positive, and it follows that η is also positive.

[26] Substituting equations (45) into (33) yields

$$\eta^2\beta^2 - \beta^2 + 2\eta\beta v_* = 0, \tag{46}$$

simplifying to

$$\beta = \frac{2\eta v_*}{1-\eta^2}. \tag{47}$$

[27] Both η and β are positive, so the sign of v_* is the same as $1-\eta$, considering the factoring of the denominator. Substituting equations (45) into (34) yields

$$\beta(\eta\beta + v_*) = 1. \tag{48}$$

Eliminating β by substituting equation (47) yields an equation with only v_* and η,

$$\frac{2\eta v_*}{1-\eta^2}\left(\eta\frac{2\eta v_*}{1-\eta^2} + v_*\right) = 1 \tag{49}$$

and simplifying

$$2v_*^2\frac{\eta}{1-\eta^2}\left(\frac{2\eta^2}{1-\eta^2} + \frac{1-\eta^2}{1-\eta^2}\right) = 1 \tag{50}$$

yields a solution for v_*^2:

$$v_*^2 = \frac{(1-\eta^2)^2}{2\eta(1+\eta^2)}. \tag{51}$$

[28] The sign of v_* is the same as $1-\eta^2$, which is the positive root. Summarizing earlier sign conventions (z positive downward) and discussion of signs, positive velocities are downwelling with $\eta < 1$, and negative velocities are upwelling with $\eta > 1$:

$$v_* = \frac{1-\eta^2}{\sqrt{2\eta(1+\eta^2)}} = \frac{1}{\sqrt{2}}\frac{\frac{1}{\eta}-\eta}{\sqrt{\frac{1}{\eta}+\eta}}. \tag{52}$$

[29] When considering the relative dominance of advective and diffusive heat transport, we can look in the limit, and note that v_* or Pe is large when either $\sqrt{\eta} \gg 1$ or $\frac{1}{\sqrt{\eta}} \gg 1$, showing that η is a direct indicator of the relative magnitude of conduction and advection.

[30] Although the first form in equation (52) may be practical in some situations, the second form on the far right side of equation (52) shows the symmetry of the solution around $\eta = 1$ in a ratio sense. Equation (52) offers a solution that is more directly related to temperature time series and does not require knowledge of the depth of instrument placement. Knowledge of diffusivity is still required to estimate the advective thermal velocity from v_*, however, and we address this below. A useful feature of equation (52) in contrast to equations (9), (10), (41), and (44) is that it is an *explicit* closed-form solution, which is to say that it does not require iterations or numerical methods for root finding to solve for v_* from field-derived variables. There are other advantages to this solution that are not as readily apparent strictly from the mathematical form.

[31] For some analyses, it is useful to be able to easily invert equation (52) and solve for η given v_*. In this case, an explicit form is readily obtained by dividing equations (41) by (44):

$$\eta = \frac{\alpha}{\beta} = \frac{\sqrt{\frac{\sqrt{v_*^4+4}+v_*^2}{2}} - v_*}{\sqrt{\frac{\sqrt{v_*^4+4}-v_*^2}{2}}} = \frac{\sqrt{\sqrt{v_*^4+4}+v_*^2} - \sqrt{2}v_*}{\sqrt{\sqrt{v_*^4+4}-v_*^2}}. \tag{53}$$

2.3.3. Completing the Solution: Estimating Diffusivity, Depth Variation, and v_t

[32] The direct correspondence between η and v_* is useful for obtaining information regarding the diffusive properties of the system because the effects of velocity can be separated from the effects of diffusion to a particular depth. Solving equation (34) for v_* and substituting into equation (33) to eliminate v_* describe the relationship between the amplitude decay rate and the phase shift rate:

$$2\frac{\alpha}{\beta} = \alpha^2 + \beta^2. \tag{54}$$

Recalling equations (26) and (27), the definitions of α and β, and equation (45), the definition of η is as follows:

$$2\eta = \left[\frac{\ln(A_r)}{\Delta x}\right]^2 + \left[\frac{\Delta\phi}{\Delta x}\right]^2. \tag{55}$$

Recalling further that Δx is the rescaled depth, containing both depth and diffusivity information (equation (15c)) and rearranging

$$\left(\frac{\Delta z}{z_d}\right)^2 = \frac{\left(\ln^2(A_r) + \Delta\phi^2\right)}{2\eta}, \tag{56}$$

which can be simplified to solve for Δz, if z_d or κ_e is known:

$$\Delta z = z_d\sqrt{\frac{\ln^2(A_r) + \Delta\phi^2}{2\eta}}. \tag{57}$$

[33] Equation (57) is particularly useful for tracking scour and aggradation over time once z_d, a relatively constant

characteristic in time, has been estimated. Equation (56) can also be solved for z_d, and thereby κ_e, if Δz is known:

$$z_d = \Delta z \sqrt{\frac{2\eta}{\ln^2(A_r) + \Delta\phi^2}} \tag{58}$$

and

$$\kappa_e = \frac{\eta\omega\Delta z^2}{\ln^2(A_r) + \Delta\phi^2}. \tag{59}$$

[34] Applying equations (14) and (20) with (52) and (58) yields an expression for estimating the advective thermal velocity directly from observations of depth and temperature:

$$v_t = \frac{\omega\Delta z}{\sqrt{\ln^2(A_r) + \Delta\phi^2}} \frac{1-\eta^2}{\sqrt{(1+\eta^2)}}. \tag{60}$$

[35] Taken together, equations (59) and (60) provide estimates of the two parameters for the original PDE (3). If diffusivity information for a particular set of measurements is deemed more reliable than the depth measurements for some reason, equation (57) could be substituted into equation (60) yielding

$$v_t = \frac{\omega z_d}{\sqrt{2\eta}} \frac{1-\eta^2}{\sqrt{(1+\eta^2)}}. \tag{61}$$

[36] Equation (54) can also be rearranged to provide estimates of α and β individually as functions of η (meaning that no depth or diffusivity data are required), which can be useful for directly providing the parameters for equation (24); the two equations are as follows:

$$\beta = \sqrt{\frac{2}{\frac{1}{\eta} + \eta}} \tag{62}$$

and

$$\alpha = \beta\eta = \eta\sqrt{\frac{2}{\frac{1}{\eta} + \eta}}. \tag{63}$$

[37] Equations (62) and (63) may also be used to estimate the depth of a sensor, diffusivity, or thermal velocity in a fashion similar to that outlined following equations (55)–(60) by drawing on equations (26) and (27):

$$\Delta z = \Delta\phi z_d \sqrt{\frac{\frac{1}{\eta} + \eta}{2}} = \frac{-\ln(A_r) z_d}{\eta} \sqrt{\frac{\frac{1}{\eta} + \eta}{2}}, \tag{64a}$$

$$z_d = \frac{\Delta z}{\Delta\phi} \sqrt{\frac{2}{\frac{1}{\eta} + \eta}} = \frac{\eta\Delta z}{-\ln(A_r)} \sqrt{\frac{2}{\frac{1}{\eta} + \eta}}, \tag{64b}$$

$$\kappa_e = \frac{\omega\Delta z^2}{\Delta\phi^2\left(\frac{1}{\eta} + \eta\right)} = \frac{\omega\eta^2\Delta z^2}{\ln^2(A_r)\left(\frac{1}{\eta} + \eta\right)}, \tag{64c}$$

$$v_t = \frac{\omega\Delta z}{\Delta\phi}\left(\frac{1-\eta^2}{1+\eta^2}\right) = \frac{\eta\omega\Delta z}{-\ln(A_r)}\left(\frac{1-\eta^2}{1+\eta^2}\right). \tag{64d}$$

[38] Although equations (9) and (10) are known for yielding sometimes disparate answers for v_t based on amplitude ratios or phase differences, equations (57)–(60) and (64a)–(64d) can be expected to provide the same estimates of depth, diffusivity, or velocity. Equations (9)–(12) isolate phase information and amplitude information and use an independent estimate of κ_e. If the estimate of κ_e is incorrect, the equations will disagree. Equations (41) and (42) can have the same issue. Equations (57)–(60) and (64a)–(64d) use the η parameter, so contain both pieces of information in different algebraic arrangements and do not require an a priori estimate of κ_e. Although rescaling the PDE (3) was useful for deriving the final set of equations, note that equations (57)–(60) and (64a)–(64d) do not use nondimensional variables and can be applied directly from analysis of temperature records.

3. Visualizing the Solutions

[39] By nondimensionalizing, we create a single "type curve" between η, which is derived fairly directly from temperature measurements, and dimensionless velocity, v_* (Figure 2). The type curve can be rescaled by the diffusive phase velocity, v_d, to estimate the advective thermal velocity, v_t. The relationship between η and v_* is similar in character for η and $1/\eta$, so is best displayed with η on a log-scaled axis. The relationship is symmetric around $\eta = 1$, $v_* = 0$ (Figure 2).

[40] An altered form of upper left quadrant of this graph has been shown before. *Stallman* [1965] introduced the ratio a/b as part of a tabular/graphical solution technique

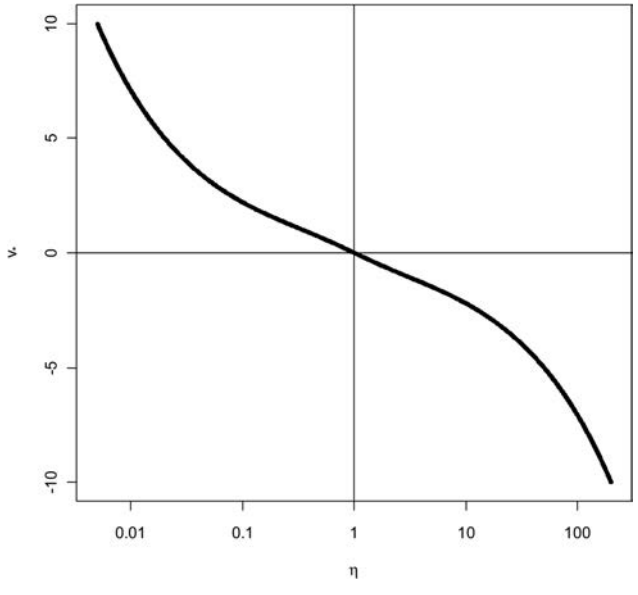

Figure 2. Relationship between η and v_*. η axis is log scale.

for v_t and z_d. The graph presented there has very similar underlying information, being essentially a plot of η as a function of $2v_*$; however, the log scale being on the $2v_*$ axis instead of the η axis obscures some of its significance, particularly in giving the false appearance of an asymptotic relationship as η approaches 1. Stallman's [1965] graph was derived from an analog to our equation (53), and the graph was used to invert it to find v_* from η. The explicit solution in equation (52) obviates the graphical step, but a basic procedure, relating both diffusive and velocity parameters to a and b, was outlined with the graphical solution.

[41] Figure 3 shows the sensitivity of v_* to ratio changes in η. The sensitivity of v_* is lowest at low velocities, where a 1% increase in η yields a change in v_* between 0.009 and 0.01. At higher velocities, a ratio change in η yields a ratio change in v_*, so that a 2% increase in η corresponds to a 1% increase in v_*. This is a fairly practical sensitivity behavior for estimation so that velocities near zero can be found with reasonable precision, whereas larger velocities are bounded in percentage error. We apply this unique form of sensitivity, looking at the change in v_* per unit change in $d\eta/\eta$ because of this semi-log behavior. For values of η near 1, v_* is nearly linear in $\log(\eta)$ (Figure 2), suggesting this form, whereas, at the extremes, the relationship between v_* and η looks like $v_* \propto \sqrt{\eta}$ for large η, and $v_* \propto 1/\sqrt{\eta}$ for η approaching 0, again giving this form utility by highlighting the constant ratio sensitivity with the straight lines.

[42] The equations describe a complete set of relationships among η, v_*, amplitude ratio changes with depth, and phase changes with depth (Figure 4). What is generally unappreciated in solutions where information about log-amplitude ratio or change in phase is used independently is that the relationship among them is constrained. The relationship between v_* and η is a new equation that describes

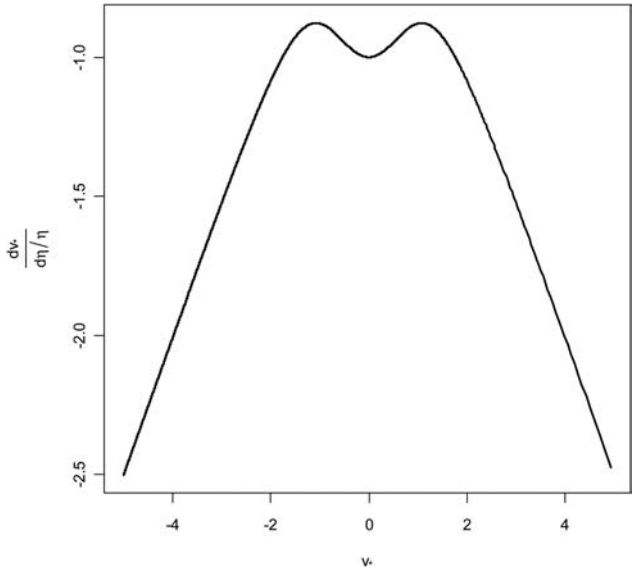

Figure 3. Sensitivity of v_* to ratio changes in η. Where the curve is straight, it implies constant proportional sensitivity where a 2% increase in η yields a 1% increase in v_*. For smaller absolute values of v_*, a 1% change in η yields a change in v_* of between 0.009 and 0.01.

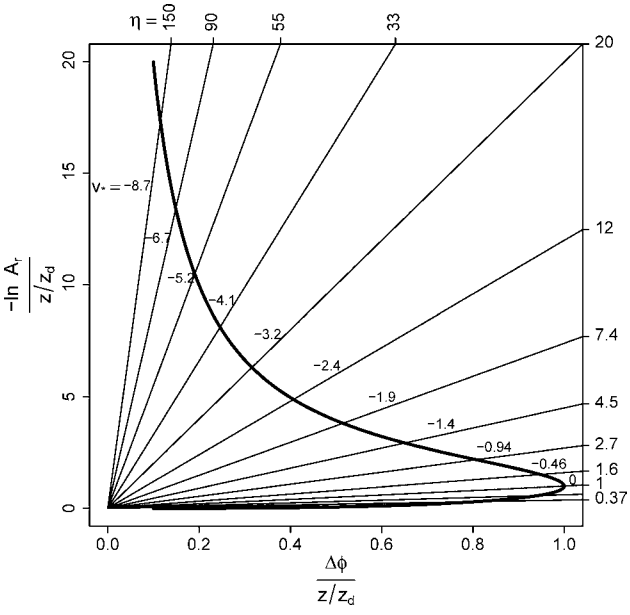

Figure 4. The relationship between $\Delta\phi$ and $\ln(A_r)$ scaled by nondimensional depth as η or v_* (on the labeled lines) varies. The key point is that $\ln(A_r)$ and $\Delta\phi$ are not independent, but rather that, for a specific location (set diffusivity and depth), one is specifically related to the other by the fluid velocity. This image shows essentially the half space for $\eta > 1$, while the portion of the relationship for $0 > \eta > 1$ is greatly compressed. If the y axis is plotted on log scale they appear approximately symmetrical, but the lines of constant η become curved.

this relationship, enabling further extraction of information from measurements (e.g., we now have two equations in two unknowns). Note that lines of constant η and v_* intersect the A_r versus $\Delta\phi$ curve to specify uniquely where along that curve a set of observations lie, and that curve could be specified as a parametric curve in v_* or η. This unique situation can be attributed to the diurnal variation boundary condition, which changes the characteristic length scale of the problem from the fixed physical depth of observation usually applied in advection-diffusion analysis to a depth related to the phase velocity of the diurnal temperature wave and the characteristic time scale of 1 day, which links the phase and amplitude, and gives depth an independent influence in the context of the relationship between the amplitude ratio and phase. The relationship is shown for $\ln(A_r)$ against $\Delta\phi$, each per unit of dimensionless depth. Although the curve is not quite symmetric if the y axis is plotted as $\log(\ln(A_r))$, the lines of constant η and v_* would not be lines but curves; so this plot is essentially looking at half of the picture. The asymmetry is just a consequence of the relationship among η, β, and α, and β is symmetric in η.

[43] The coupling of A_r and $\Delta\phi$ in ways that can be scaled with depth demonstrates that any two time series of temperature taken from two different depths can tell us whether the flow is downwelling, neutral, or upwelling. Figure 5a shows a close up of the surface temperature variation and the potential subsurface temperature variations

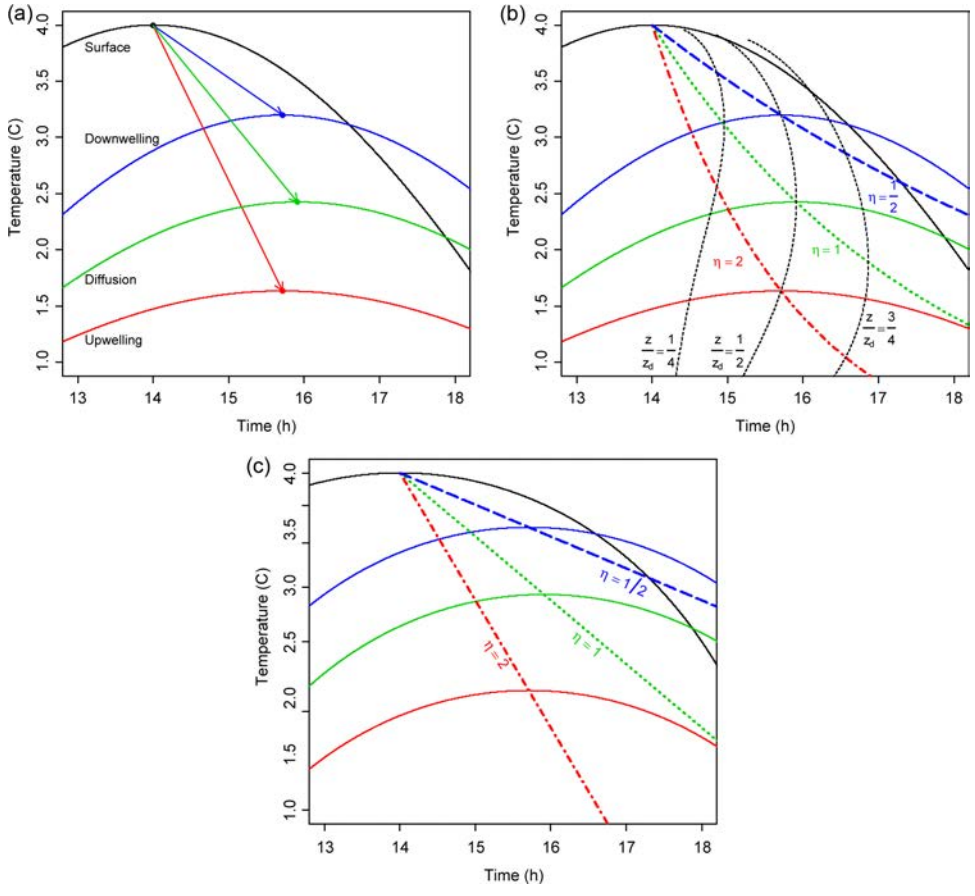

Figure 5. (a) Hypothetical relative movement of the diurnal signal through the profile showing the relative shape of the temperature wave at depth under downwelling, neutral, and upwelling conditions at a depth that is half of the diurnal damping depth. The arrows show the relative movement of the crest of the diurnal signal, which peaks at 14:00 at the surface. (b) Same temperature traces as in Figure 5a overlain with characteristic curves for motion of a point of constant phase (e.g., the crest of the diurnal signal) for constant η in blue, green, and red, and for constant z/z_d in black. The η characteristics show the path of the crest for a range of depths, whereas the black curves show the size and timing of the crest at a given depth for a range of velocities. Note that the curves for η have no other parameters and are also curves of constant v_*. The dashed curves in black are parameterized by the diffusive damping depth (where the amplitude at depth would be $1/e$ the amplitude at the surface under diffusive conditions), which depends on the diffusivity. The three temperature traces from Figure 5a have a crest where their respective characteristics cross the curve for $z = z_d/2$. (c) Same temperature traces and η characteristics as in Figure 5b with the temperature anomaly axis on a log scale, rendering the η characteristics as lines.

depending on flow conditions: downwelling, neutral, or upwelling. Upwelling flows further dampen amplitude of the diurnal cycle, because the diffusive front is fighting the current. The upwelling condition serves to sharpen the temperature gradient, allowing diffusion to carry information to depth against the current. However, this condition causes the amplitude information to diffuse rapidly, and amplitudes at even relatively shallow depths can be damped so strongly as not to be practically observable for large upwelling velocities. Downwelling flows carry information about the surface boundary condition to depth more rapidly than under diffusive conditions; so amplitudes are greater at depth and occur sooner than under purely diffusive circumstances. Phase differences and amplitude ratios can become indistinguishable for small depth changes or high velocities. A more detailed examination of the curves in Figure 5a shows that curves of constant η can be drawn emanating from the crest of the surface temperature wave, with initial temperature, T_i, and propagate as

$$T - T_i = Ae^{-\eta\omega t} \tag{65}$$

to show the progressive position of the crest, as one goes deeper (Figure 5b). These serve as characteristic curves along which

$$\frac{\mathrm{d}U}{\mathrm{d}\tau} = -\eta e^{-\eta\tau}. \tag{66}$$

[44] Along these curves, then, equation (21) is a linear second-order ordinary differential equation in depth with

known parameter v_*. Here, they are plotted starting at the crest, but they could conceptually start anywhere along the surface temperature trace to plot the trajectory of that particular phase. Normally, method of characteristic solutions are applied to find possible analytical solutions along characteristics, for example, for position along each curve with depth, but we already have that analytical solution in terms of slight modifications to equations (57) and (64a), which offer the position along each curve as a function of dimensionless depth given $\ln(A_r)$ or $\Delta\phi$. Intersecting curves showing how the amplitude and phase of the crest vary over a range of velocities for a fixed dimensionless depth are also shown in Figure 5b. When depths are known, we can use them to estimate the thermal diffusivity parameter.

[45] Understanding the three different metrics is useful as well. From equation (24), we see that β is the wave number of the diurnal wave; so, β is the number of cycles (days) per unit of rescaled depth. We can also note that if we follow a constant phase,

$$\frac{\mathrm{d}}{\mathrm{d}t}(\omega t - \beta x) = 0 \tag{67}$$

and

$$\frac{\mathrm{d}x}{\mathrm{d}t} = \frac{\omega}{\beta}. \tag{68}$$

[46] Recalling the rescaling of z to x, we can see that the phase velocity, v_p, of the diurnal wave under nondiffusive conditions is

$$v_p = \frac{\mathrm{d}z}{\mathrm{d}t} = \frac{v_d}{\beta} \tag{69}$$

so that $1/\beta$ provides a scaling of the diffusive phase velocity for the nondiffusive case. The phase velocity is always positive, so always downwelling into the bed, even when fluid is upwelling. This may look more like a "thermal front velocity" into the bed than does the advective thermal velocity, particularly given that propagation of thermal variations from the stream into the bed occurs even when v_t is out of the bed. Note that there are no conditions where v_p would be expected to be equal to v_t, because both conductive and advective processes are taking place simultaneously. For further insights, we can draw on equations (34) and (69) to write

$$\alpha\beta = 1 - \frac{v_t}{v_p}. \tag{70}$$

Equations (62) and (63) serve to replace the left-hand side:

$$\frac{2\eta^2}{\eta^2 + 1} = \frac{v_p - v_t}{v_p}. \tag{71}$$

Knowing the signs and relationships discussed earlier (meaning we are not dividing by 0), we can invert both sides and separate the left-hand side:

$$1 + \frac{1}{\eta^2} = \frac{2v_p}{v_p - v_t}. \tag{72}$$

Simplifying and inverting again, we can relate η more directly to the phase velocity and advective fluid velocity:

$$\eta = \sqrt{\frac{v_p - v_t}{v_p + v_t}}, \tag{73}$$

providing further insights into the relationship between v_p and v_t, such as

$$|v_p| > |v_t|. \tag{74}$$

[47] Equation (74) seems fairly reasonable under downwelling conditions when the phase velocity and fluid velocity are in the same direction, but it seems more remarkable for upwelling conditions when they are in opposite directions. This relates to the sharpening of the temperature gradient discussed in an earlier paragraph. The phase velocity, though, is just the speed that information about variations in the upper boundary condition propagates into the bed. That needs to be paired with information about how rapidly the information (amplitude) is degrading.

[48] From equation (24), α is fairly readily recognized as the scaling of the depth for the nondiffusive case relative to the diffusive case and represents the number of Napierian log cycles (e.g., a division of amplitude by e) per unit of rescaled depth. The division of α by β then represents ratio changes in amplitude per unit depth divided by the number of cycles per unit depth. Because the frequency is fixed, the number of cycles is a measurement of time, and equations (1) and (45) describe η as the "velocity" of the log amplitude. If we rescale Figure 5b to have a log axis for the temperature anomaly, curves of constant η become straight lines (Figure 5c). Although the units on the sides of Figure 5c are hours and degrees, η represents the number of Napierian log cycles of amplitude per radian of a daily cycle. With a 24 h period, a radian represents about 3.82 h. An η of 1 is equivalent to a halving of amplitude approximately every 2.65 h.

[49] Calculation of η does not require knowledge of any parameters of the system, nor the actual position of sensors; so, the signatures of downwelling, neutral, and upwelling flows are fairly readily seen in temperature traces from two depths (Figure 6). In Figure 6, having a reference figure for $\eta = 1$ makes the contrasts fairly easy. Alternatively, one or several characteristic curves placed on the graph with $\eta = 1$ could facilitate comparisons given pair of time series.

4. Sensitivity to Errors in A Priori Estimates of Diffusivity

[50] Although the equations presented here show how both thermal diffusivity and Darcian velocity can be found from temperature traces at known depths, previous solution methods required an a priori estimate of diffusivity to solve for velocity (see, for example, discussion in *Hatch et al.* [2006]). We present contrasting sensitivity of different solution approaches to a priori thermal diffusivity estimates, because it gives insights about the potential for the η-based solution to provide robust estimates of velocities near 0.

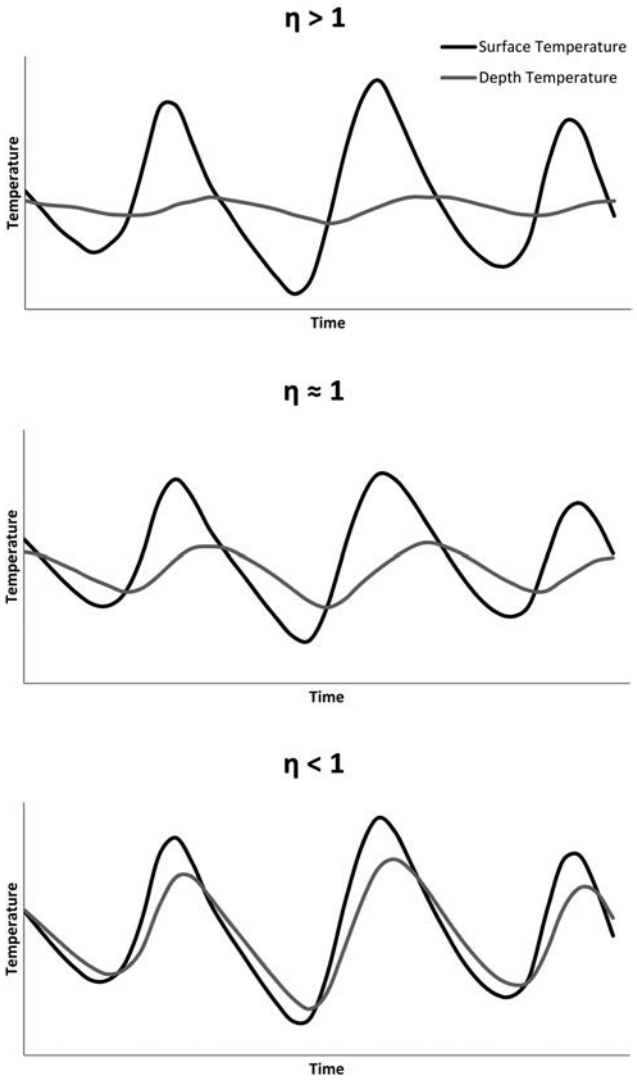

Figure 6. Examples of observed temperature traces (from *Gariglio* [2012]) at surface and at depth for upwelling ($\eta > 1$, $v_* < 0$), neutral ($\eta \approx 1$, $v_* \approx 0$), and downwelling ($\eta < 1$, $v_* > 0$) conditions.

Using only the log-amplitude ratio to estimate velocity based on an a priori estimate of thermal diffusivity can result in predicting nonzero velocity, when, in fact, there is no velocity (Figure 7a), and, as a corollary, it is likely to produce large percentage errors in velocity for small velocities. In Figure 7a, two curves are drawn, one for a "true" diffusivity of 5×10^{-6} m^2 s^{-1} and one 20% smaller. For this shift, there is a shift of about 0.03 in units of $\ln(A_r)$ or about 11%, for $v_t = 0$. In the neighborhood of the intercept of the "true" curve with zero velocity, percentage errors are substantial, and over the range between the two estimates where $\ln(A_r)$ intercepts zero velocity, percentage error in velocity is essentially undefined. This would suggest that, unless κ_e is known with precision, identifying the sign of flow direction or the magnitude of small velocities could be in error when using equation (9).

[51] The effects of errors in thermal diffusivity on estimates of velocity from phase differences are more complex. Phase differences are not currently used to estimate velocities near zero, because the curve relating $\Delta\phi$ and v_t is steep near $v_t = 0$. Nonetheless, there is utility in understanding the sensitivity. Shifting the "true" value to 4.5×10^{-6} m^2 s^{-1} allows contrast of both underestimates and overestimates as well as a look at the magnitude of a similar shift as was used for Figure 7a. If thermal diffusivity were overestimated, there would be a small range of $\Delta\phi$ for which equation (10) would not be able to estimate a velocity, after which velocity would generally be underestimated (Figure 7b). If velocity is taken as 0, in the range where the $\Delta\phi$ value is not admissible, then substantial underestimates would occur over that range. If thermal diffusivity is overestimated, there is no value of $\Delta\phi$ for which zero velocity would be estimated, and velocities would be overestimated. As is already well appreciated, phase change is a poor way to find zero velocity or estimate small velocities [e.g., *Lautz*, 2010]. However, for large velocities, errors appear to asymptotically decrease. The span of $\Delta\phi$ between the red and blue lines represents about 7 min, and the relative sensitivity of the phase equations to the amplitude equations for small changes in the independent variable can be seen by contrasting Figures 7a and 7b.

[52] In contrast to the other approaches if an a priori estimate of κ_e is applied, the η-estimated velocity near zero shows little error (Figure 7c). Zero velocity is found at $\eta = 1$ regardless of the value of κ_e. Errors in velocity as one departs from zero velocity are only square-root dependent on the error in κ_e, and it is worthwhile to note the relative magnitude of errors in Figures 7a and 7c despite a similar velocity range and slightly larger relative range in η in Figure 7c than in $\ln(A_r)$ in Figure 7a. This means that if Δz is not known and κ_e cannot be identified from measurements, the measured η can still be used to reliably determine the direction of flow, and an independent estimate of κ_e will yield less error in v_t than would be expected from other approaches for small flows. The utility of the approach might be most fully appreciated in circumstances where seasonal dynamics of flows are being examined, and flows may change from upwelling to downwelling, as the groundwater aquifer changes configuration, for example. Although we provide an example here for one discrete change in thermal diffusivity, the theoretical foundation provided in the next section allows for a continuous representation of the effects of uncertainty in thermal diffusivity.

5. Sensitivity to Measurement Errors

[53] Previous solutions of the vertical hyporheic fluxes, $q = v_t\gamma$, derived from segregated analysis of the phase and amplitude of the temperature signal have an implicit function form, and recursive or iterative numerical methods are required to find a solution. Consequently, the analysis of the propagation of the uncertainties associated with measurement errors and parameter estimations on hyporheic fluxes (magnitude and direction) relies on sensitivity analysis or methods such as Monte Carlo simulations [*Gordon et al.*, 2012; *Saltelli et al.*, 2004; *Shanafield et al.*, 2011]. Conversely, the uncertainty of a quantity, f, which is an explicit function of n parameters, x_i, with $i = 1, 2, \ldots, n$, due to their uncertainties expressed as variance, σ_i^2, and covariance σ_{ij}, can be quantified with the following

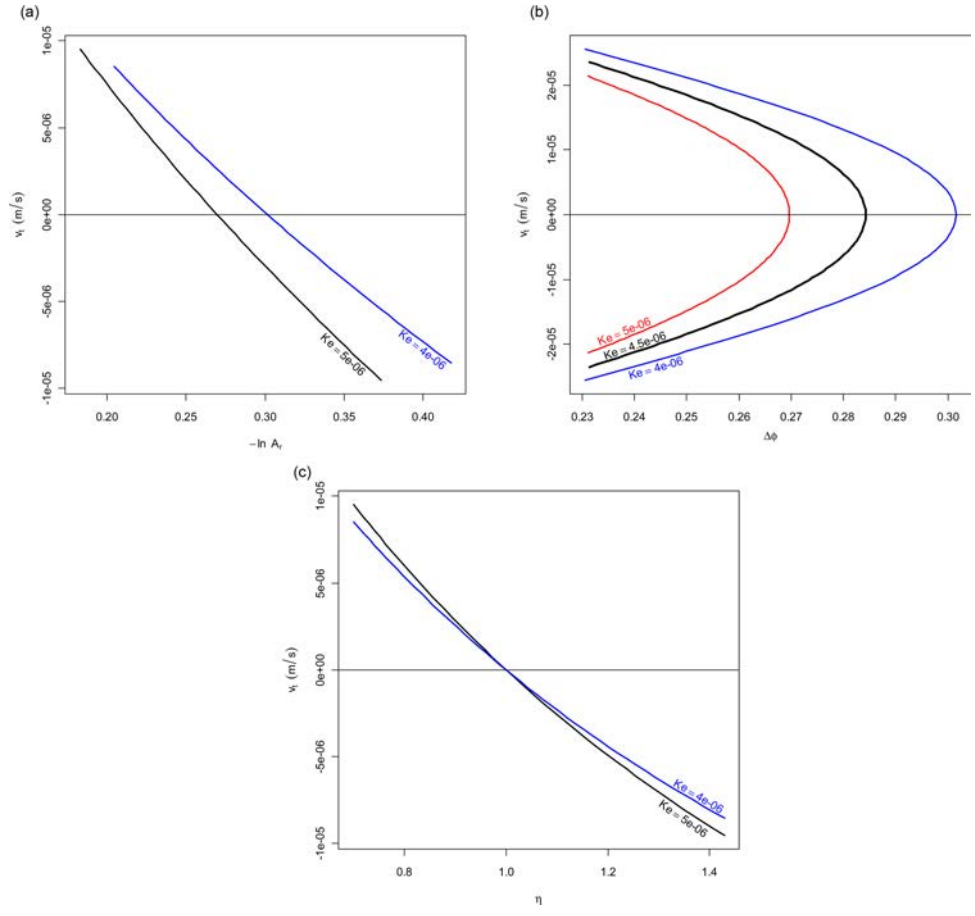

Figure 7. (a) Differences in the relationship between the advective thermal velocity and the amplitude ratio for a change in diffusivity. (b) Differences in the relationship between the advective thermal velocity and the phase difference for a change in diffusivity. Note that the v_t axis ranges between $\pm 1e^{-05}$ in Figures 7a and 7c when comparing. (c) Differences in the relationship between the advective thermal velocity and the η for a change in diffusivity.

equation [*Arras*, 1998; *ISO/IEC Guide 98-3*, 2008; *Ku*, 1966]:

$$\sigma_f = \sqrt{\sum_{i=1}^{n} \left(\frac{\partial f}{\partial x_i}\right)^2 \sigma_i^2 + \sum_{i \neq j} \sum \left(\frac{\partial f}{\partial x_i}\right)\left(\frac{\partial f}{\partial x_j}\right)\sigma_{ji}}, \quad (75)$$

where σ_f is the standard deviation for the function f. This expression simplifies to the following equation when the parameters x_i are independent from one another:

$$\sigma_f = \sqrt{\sum_{i=1}^{n} \left(\frac{\partial f}{\partial x_i}\right)^2 \sigma_i^2}. \quad (76)$$

[54] A common limitation of this approach is that it assumes that uncertainties are normally distributed [*Saltelli et al.*, 2004]. However, errors for both time and temperature measurements in the temperature sensors are typically reported with normal distributions. If a specified confidence interval different from that associated with a standard deviation needs to be used for the uncertainty analysis, equations (75) and (76) can be modified by replacing the standard deviation, σ_i, with the uncertainty values u_A and u_ϕ with the prescribed confidence interval.

[55] Equations (45), (52), (60), and (64d) are explicit solutions of v_t, η, and v_* such that the propagation of the measurement errors of the phase (ϕ) and temperature amplitude (A) and of the uncertainty of the thermal properties of the sediment (κ_e) can be quantified with equation (75) or (76). Because sediment thermal properties, temperature amplitude, and phase measurements are independent variables, equation (76) can be adopted in this application. However, if the assumption of independence does not hold with different equipments or conditions, the same analysis can be performed with equation (75).

[56] The values of η and v_* only depend on measured temperature amplitudes and phase shifts and not on the sediment thermal properties. Thus, estimates of the uncertainty of η, σ_η, can be quantified with the following equation, which applies equation (75) for sensors at depth 1 (shallow)

and 2 (deep) each with the same errors for the amplitude error σ_A and phase error, σ_ϕ:

$$\sigma_\eta = \sqrt{\frac{\sigma_A^2}{(\phi_2-\phi_1)^2}\left(\frac{1}{A_2^2}+\frac{1}{A_1^2}\right)+2\frac{\sigma_\phi^2 \ln(A_2/A_1)^2}{(\phi_2-\phi_1)^4}}. \quad (77)$$

[57] If σ_A and σ_ϕ are known, then contour plots of the distribution of σ_η over the amplitude and phase field can be developed (Figures 8a and 9a). Figures 8a and 9a show an example of contour plots for $\sigma_A = 0.1$°C and $\sigma_\phi = 0.06$ radian (about 13.75 min). Large errors cluster near small phase shift values and small amplitude differences between sensors. Errors are large, and η curves converge in the upper right-hand corner of Figures 8a and 9a, where differences of both amplitude and phase shift are small. Thus, predictions of the hyporheic flux direction, which only depends on η values, are less certain in that section of the graph than other areas of the amplitude-phase field. Measurements from the field experiments of *Gariglio* [2012] for location A provide highly uncertain estimations of hyporheic flux directions (Figure 8a) during summer with a high flux rate. However, measurements at position B are reliable. Reliability is high at both locations in spring even when surface amplitude is small, because upwelling flux rates were not as challenging for estimating fluxes during springtime (Figure 9a).

[58] Specifying equation (76) for the standard deviation of the dimensionless advective thermal velocity, σ_{v_*}, quantifies the uncertainty on the intensity of the hyporheic fluxes:

$$\sigma_{v_*} = \frac{1}{\sqrt{2}}\sqrt{\left[\frac{-\sqrt{\eta+\frac{1}{\eta}}(\eta^4+6\eta^2+1)}{2\eta(\eta^2+1)^2(\phi_2-\phi_1)}\left(\frac{1}{A_2}-\frac{1}{A_1}\right)\right]^2\sigma_A^2 + \left[\frac{-\sqrt{\eta+\frac{1}{\eta}}(\eta^4+6\eta^2+1)}{(\eta^2+1)^2(\phi_2-\phi_1)}\right]^2\sigma_\phi^2}. \quad (78)$$

[59] Uncertainty values (σ_{v_*}) are small in the central region of the graph and increase toward high amplitudes and small phase shifts (Figures 8b and 9b) as observed in Figures 8a and 9a. Absolute uncertainties are large in upwelling areas ($\eta > 1$) but large values of v_* offset this increase in absolute error. This is illustrated by the contour plot of the coefficient of variation of v_*, defined as σ_{v_*}/v_* (Figures 8c and 9c). Figures 8c and 9c show a ridge with

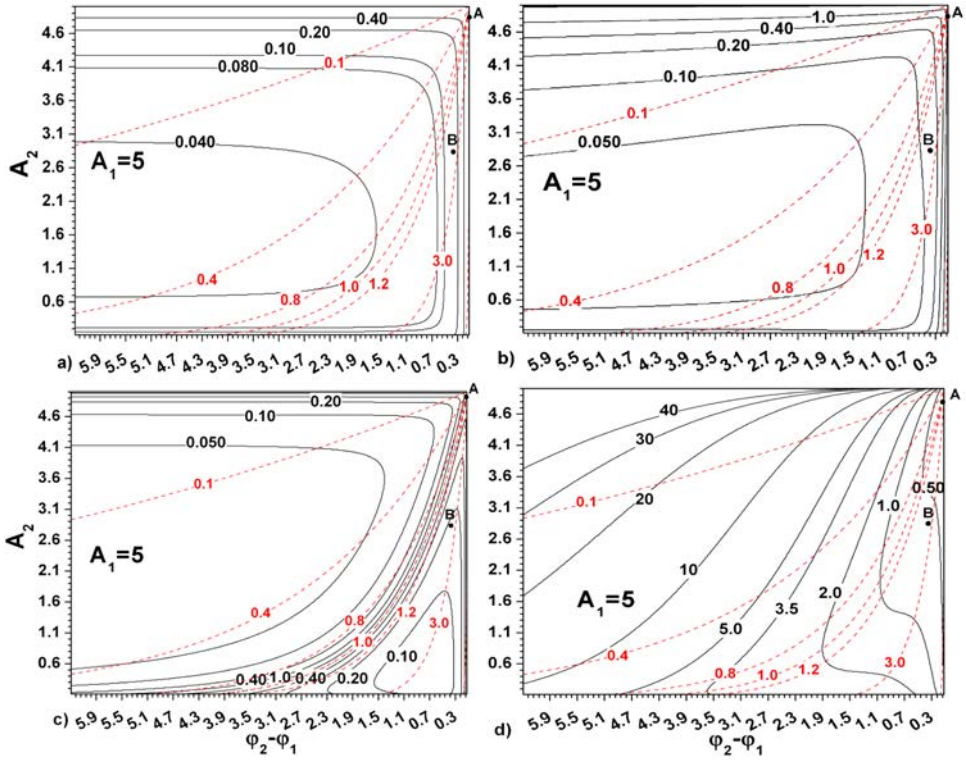

Figure 8. Solid black lines represent (a) root-mean-square error of η, σ_η; (b) root-mean-square error of the dimensionless hyporheic flux, σ_{v_*}; (c) the ratio between σ_{v_*} and v_*; and (d) $\Delta z/z_d$ as a function phase shift and amplitude of the deeper sensor with the amplitude of the shallower sensor fixed at 5°C. Red-dashed lines represent η values; the points A and B represent values at two locations in the experiment of *Gariglio* [2012] between sensors at the surface and at 10 cm deep. A_1 is the amplitude of the temperature signal (°C) at the shallow sensor and A_2 is the amplitude of the temperature signal (°C) at the deep sensor.

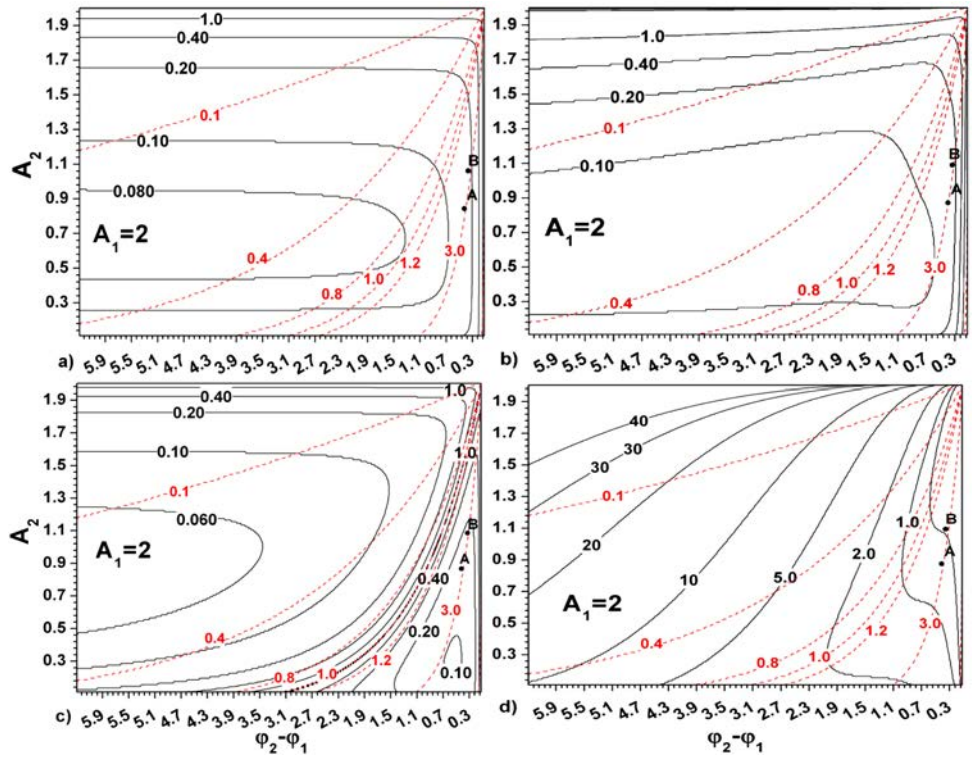

Figure 9. Solid black lines represent (a) root-mean-square error of η, σ_η; (b) root-mean-square error of the dimensionless hyporheic flux, σ_{v_*}; (c) the ratio between σ_{v_*} and v_*; and (d) $\Delta z/z_d$ as a function phase shift and amplitude of the deeper sensor with the amplitude of the shallower sensor fixed at 2°C. Red-dashed lines represent η values; the points A and B represent values at two locations in the experiment of *Gariglio* [2012] between sensors at the surface and at 10 cm deep. A_1 is the amplitude of the temperature signal (°C) at the shallow sensor and A_2 is the amplitude of the temperature signal (°C) at the deep sensor.

errors larger than 100% along the $\eta = 1$ curve. This is because hyporheic fluxes tend to zero, but errors are still finite near $\eta = 1$. However, this region of the graph around the $\eta = 1$ curve is less important for estimating advective hyporheic velocities, because diffusion dominates, and hyporheic fluxes are negligible.

[60] Interestingly, downwelling fluxes have a large area with errors below 5% (Figure 8c). This area decreases for small temperature amplitudes of the shallow sensors (cf., Figures 8c and 9c). Consequently, the reliability of this method may depend on local surface water temperature conditions. However, setting the spacing between sensors can partially offset the effects of local surface water temperature conditions and maximize the performance of this technique by minimizing the propagation of uncertainty. For instance, in areas where downwelling fluxes dominate, it would be appropriate to use spacing of $\Delta x = 10$ (recall that $\Delta x = \Delta z/z_d$), because this line would intersect low-error contour curves. However, this sensor arrangement would not be able to detect any change in flux direction. On the other hand, sensors with $\Delta x = 1$ would be able to differentiate upwelling and downwelling fluxes and still intersect contour lines with relatively low errors. Conversely, sensors that are too close, $\Delta x < 0.5$, would provide less reliable estimates. Thus, inspection of the thermal properties and thermal fluctuations of the system where the sensors are deployed may provide valuable information on designing the experimental setup. Sensors at positions A and B are approximately on the $\Delta x = 0.5$ line, which constrains the response of the sensors to move along that line (cf., Figures 8d and 9d).

[61] These methods can be applied to expand on the sensitivity to thermal diffusivity error in the previous section to provide a more continuous representation of the effects. Uncertainty on the thermal diffusivity of the sediment affects the dimensional value of advective thermal velocity, v_t ($v_t = v_* (2\omega\kappa_e)^{1/2}$). This uncertainty can be quantified with the following equation:

$$\sigma_{v_t,k_e} = v_* \sqrt{\frac{\omega}{2\kappa_e}} \sigma_{k_e}, \tag{79}$$

which shows that the error due to the uncertainty of the thermal properties is a percentage of v_*. The error depends on the inverse of the square root of the thermal diffusivity and on the square root of the angular frequency of the signal, which is fixed and equal to 1 day. The typical range of κ_e in saturated soils is between 4.42×10^{-7} and 9.2×10^{-7} m^2 s^{-1} with mean values 6.6×10^{-7} m^2 s^{-1}. If we assume that the uncertainty around the mean values is $\sigma_{ke} = 2.44 \times 10^{-7}$ m^2 s^{-1}, the error on v_t is 13.03%

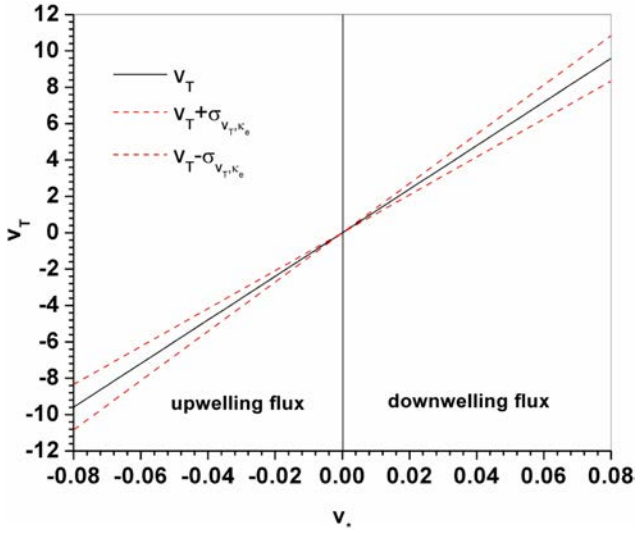

Figure 10. Propagation of the uncertainty of the effective thermal diffusivity on the advective thermal velocity uncertainty.

of v_*, and its effect on v_t can be plotted as a function of v_* (Figure 10).

6. Tracking Bed Scour Over Time

[62] Because the distance between sensors offers an independent piece of information from η, measurements of diurnal temperature variations also provide the opportunity to measure changes in the streambed above a sensor. With one sensor in the water column, measuring the surface boundary condition and a second sensor buried at depth, variations in depth to the sensor can be tracked using equation (57) or (64a). Over the period that scour is tracked, κ_e must be assumed unchanging and depth invariant. It can be estimated from a time period when Δz is known.

[63] When using the phase change or amplitude ratio equations (9) and (10) to estimate flow direction and velocity assuming constant Δz, substantial errors may be generated if bed movement changes the amount of bed material between two sensors. Figure 11a shows velocity estimates using three approaches from the downstream pool site of *Gariglio* [2012], who derived a time series of phase and amplitude of the temperature time series at the surface and at (nominally) 10 and 20 cm depth using dynamic harmonic regression in the Captain Toolbox [*Taylor et al*., 2007]. One velocity estimate was obtained based on η per equation (52) and an estimate of κ_e from a time when depth was known; another was derived based just on equation (9), where the amplitude ratio indicated both direction and velocity, and a third was calculated using the flow direction indicated by the amplitude ratio, but a velocity determined from the phase change and equation (10). While the η-based velocity shows comparatively little variation in velocity and is generally downwelling, the amplitude-based and phase-based velocities show strongly divergent patterns in velocity starting in mid-April. Although it is tempting to consider such a pattern as being caused by poor parameter estimates applied within equations (9) and (10), the η-based velocity

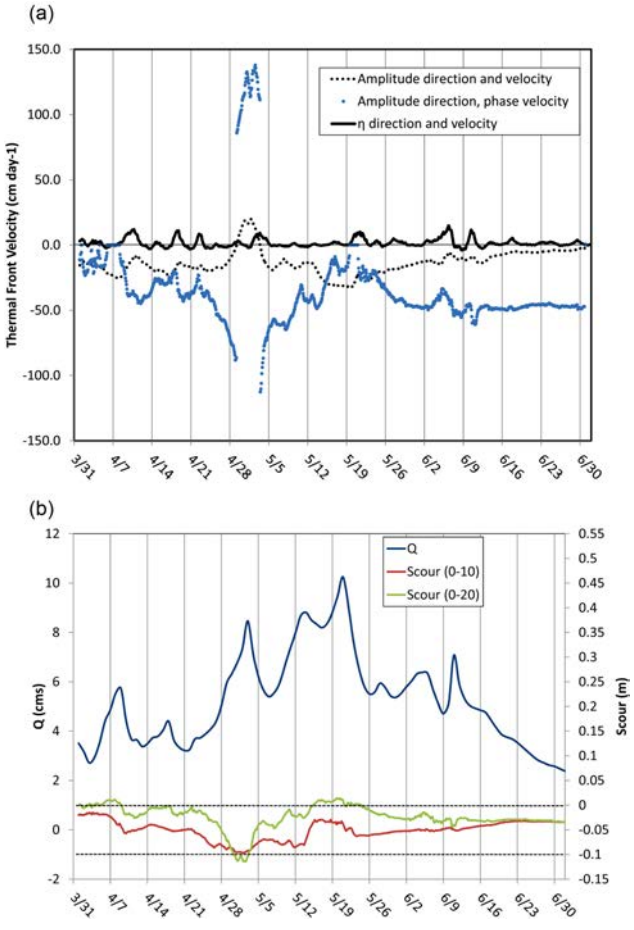

Figure 11. (a) Velocity over time estimated from one sensor at the surface and another placed 20 cm below it using three procedures: (1) using equation (9) to determine flow direction and velocity, (2) using equation (9) to determine direction and equation (10) to estimate velocity, and (3) using η to estimate direction and velocity (equation (60)). Note that when the actual fluid velocity is nominally constant but the amplitude ratio decreases, the phase shift increases, which can lead to opposite estimates in the magnitude of velocity depending on the direction of the misestimation and the direction of flow. Note also the few instances where the phase did not yield a real root, so was estimated at zero velocity. (b) Estimated scour (from equation (57)) at the downstream pool location using the surface temperature sensor and sensor placed 10 and 20 cm below it plotted with an estimated hydrograph for the site. The hydrograph is estimated from the nearby Valley Creek gage station (13295000) based on a historical relationship with the gage on Bear Valley Creek near Cape Horn (13309000) rescaled to the basin area of site [*Gariglio*, 2012].

is not affected (except in the scaling of the left axis) by estimates of κ_e. Figure 11a then focuses our question to ask why estimates from equations (9) and (10) would show marked and divergent changes despite comparatively minor fluctuations in the actual velocity.

[64] The only time-varying process that is consistent with all of these patterns is that the bed elevation dropped

and refilled. The downstream pool area contained sand to some unknown depth, so it is a physically reasonable explanation as well. Figure 11b shows a scaled reconstructed hydrograph (based on a relationship between a historical downstream gage and a modern gage in an adjacent basin) along with the imputed scour from equations (57) and (64a) based on the difference in the time series at the surface and the time series at either 10 or 20 cm below the first sensor. The general timing of the estimated scour is consistent with the hydrograph. Although there are qualitative similarities to the more abrupt changes in estimated scour based on the 10 and 20 cm sensors, the temporal pattern from the 10 cm sensor matches expectations of sediment transport better, and the disagreements may be related to heterogeneity (sand versus gravel) in sediments above and between the sensors. The analysis would be less speculative if there were direct measurements of bed elevation in the pool, but because there are so few degrees of freedom in the factors affecting bed temperature, there is value in presenting the example to encourage further investigation. In addition, this case provides a concrete example of how the η-based analysis provides additional utility in interpreting temperature time series from streambeds.

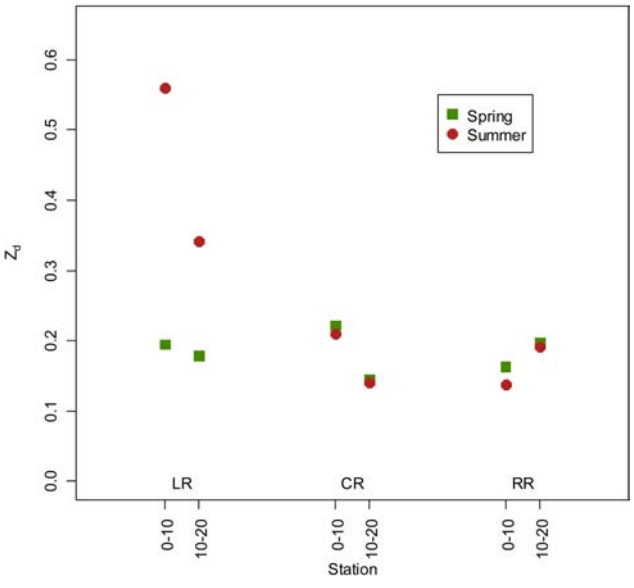

Figure 12. Damping depth estimates at three wells for spring and summer. The physical separation of the sensors was nominally 10 cm $\pm$ 1 cm except at LR, where $\sim$3 cm of sediment was scoured around the well during spring flows. For reference, when $z_d = 0.2$, $\kappa_e = 1.45 \times 10^{-6}$.

7. Validation

[65] We can test how well these equations can be used to characterize hyporheic properties from a fairly natural experiment. As flows and temperatures change in a stream over time, we expect fluid velocity as well as the magnitude of the surface boundary conditions to change, but we would expect the diffusive properties of the streambed to remain relatively constant. One test of the equations is whether the estimate of z_d stays constant across seasons despite substantial changes in temperature and sometimes streambed fluxes. Equivalently, one could do this with κ_e estimates; we chose z_d comparisons to allow for easier presentation of uncertainty.

[66] We looked at data from three wells arrayed across a riffle from the *Gariglio* [2012]. Comparison of z_d values estimated from a period during the spring and a period during the summer for three wells with sensors at nominally 0, 10, and 20 cm below the streambed surface is shown in Figure 12. One well had scour of about 3 cm near the surface, which may contribute to the error, but the measurements there illustrate potential theory or measurement errors even at depths below the scour, so we include it in this discussion. Recall that the sensor separation was approximately 10 cm, and values of z_d are between 15 and 20 cm; so errors of damping depth should be on the order of 1.5–2 times the accuracy of the physical measurement of actual depth, which was O(1 cm), assuming that Δz is the most likely source of error. For most of these measurements, there is good agreement between spring and summer estimates of z_d despite a 1.5–2°C change in the surface temperature amplitude, slight changes in hyporheic fluid velocity, and substantial changes in the stream flow.

[67] During summer, the site labeled "LR" (left riffle) experienced large downwelling velocities, and both phase and amplitude differences were very small. The large difference in estimated damping depth could be a result of instrument error. However, errors at both depth increments could not be simultaneously satisfied by errors in one instrument, so the errors could relate to deficiencies in the theory as well. Two potential examples are that (1) near the stream bank, horizontal flow exchanges are large enough to substantially affect the amplitude or timing [e.g., *Lautz*, 2010], or (2) at high velocities, the assumption that water and sediment temperatures are the same at a particular depth may be violated, particularly if large clasts are present. More specifically, the equations do not require sediment and water temperatures to be the same; however, the equations estimate the average temperature of sediment and water, and we measured the water temperature. It would be complex to assess the first issue, particularly with the paucity of independent measurements at this site; however, the second mechanism would be consistent with the direction of the observed differences, where the larger rocks would not pull as much heat from the passing water making it appear that the heat was diffusing downward faster than the velocity would account for. The site has a large Peclet number, $Pe \approx 5.1$, and the sensitivity to measurements as outlined in Figures 8 and 9 is such that one would question whether the measurements taken were suited to those particular conditions as well. Indeed, the measurement with larger separation did show better performance. The measurements were not taken with the intention of validating the equations, nor were they taken with benefit of the understanding provided in the preceding section on measurement errors. The key ideas taken from this validation exercise are (1) that the new equations outlined here provide a ready method to check measurements and (2) that comparison of these equations with more precise and complete measurements, particularly measurements that could independently verify them, could be illuminating in finding limits to their applicability.

8. Summary and Potential Applications

[68] Significant accomplishments have been made with respect to using temperature time series to estimate hyporheic fluxes over the last decade [*Constantz*, 2008; *Hatch et al*., 2006; *Keery et al*., 2007]. Drawing from this and earlier work, we present refinements that provide explicit analytical solutions as well as further insights on the relationships between measurements and system characteristics. Among other benefits, the solutions presented here should perform better than previous solutions for identifying low-flow velocities, and thus the direction of flow. At higher flow velocities, instrument precision may become limiting in identifying streambed parameters. The effects of imprecisions in boundary conditions are uncertain for this approach. There are clearly opportunities in testing limits of this solution approach with high-precision field observations and numerical solutions to more fully understand the limits of using these approximations, as others have done with previous approaches.

[69] The explicit analytical form of the η-based solution allows using an analytical procedure for uncertainty propagation. This is an important advantage because it allows quantification of the uncertainty of each prediction of flux magnitude and direction based upon a specified confidence interval for amplitude and phase estimates. This is not possible with previous solutions, which depend on numerical sensitivity analysis. Analysis of the error propagation shows that this technique is reliable in predicting hyporheic flux direction even with small temperature amplitude for the shallow sensor. This would allow the applicability of the model during springtime in temperate regions or in cold regions. However, this technique may be most reliable during summer periods or in semiarid regions such as those presented for estimating recharge on alluvial fans [e.g., *Constantz*, 2008; *Constantz and Thomas*, 1996, 1997; *Constantz and Stonestorm*, 2003; *Constantz et al*., 1994]. In those environments, this technique would quantify losses and recharges and relative uncertainty associated with those values.

[70] The capacity to estimate the diffusive properties when Δz is known represents a tremendous increase in the value of applying temperature-time-series-based solutions to hyporheic temperature data. At the most basic level, the additional equation presents the capacity to accurately estimate bulk fluid velocity free of the errors encountered with previous methods where a priori estimates of thermal diffusivity were required. Perhaps more importantly, because κ_e is conceptually a time invariant property, multiple measurements in an area or over time offer some opportunity for validation of measurements and estimates of velocity. Knowledge of diffusive properties could also be viewed as a control on interpreting measurements from multiple time periods. For example, temperature measurements from an imprecise instrument with other benefits such as cost or spatial/vertical coverage (e.g., high-resolution distributed temperature sensing (DTS) as applied in *Briggs et al*. [2012]; *Vogt et al*. [2010]) could be bias corrected, say through a Bayesian data assimilation procedure, to match the diffusive properties from an earlier period when conditions were less challenging for measurements.

[71] The lack of sensitivity of η to sensor position in the bed creates new opportunities for measuring subsurface flow velocity and other system variations using temperature time series. We discussed the potential utility for measuring bed scour when η is used to constrain potential causes for excursions of either the amplitude or phase based velocity estimates. The new analytical methods would further allow the possibility of measuring the direction of flow within redds of sensitive species by letting instruments be buried by the fishes with gravel and eggs. Regulatory constraints prohibit installation of wells with carefully measured depths within existing redds but would not prevent dispersal (and postemergence retrieval) of relatively inexpensive temperature sensors in areas where redds are being built. The insensitivity of the velocity instrument to imprecise sensor location also improves the capacity to use a tool like DTS cables, such as are already used to measure bed surface temperatures [e.g., *Selker et al*., 2006; *Westhoff et al*., 2011], to be buried to only approximately known depths and estimate fluxes over large areas or reaches of stream with substantial spatial detail. Such an approach could be made even more powerful with a small array of higher precision point sensors with known depths to quantify the diffusivity field. An experiment of this nature would go a long ways toward the challenge of bridging the gap between reach and catchment scale understanding of hyporheic exchange [*Bencala et al*., 2011; *Buffington and Tonina*, 2009; *Jencso et al*., 2009; *Lautz and Ribaudo*, 2012; *Wondzell*, 2011].

[72] There are many useful applications for spatially and vertically distributed κ_e and v_t measurements with validation and error estimates, particularly with respect to the mixed measurement or analytical methods being brought to bear on hyporheic analysis. The estimates of κ_e from this one-dimensional sinusoidal analysis could, for example, be used to provide initial estimates of the velocity and diffusivity fields for more complex numerical solutions. Measurements of the spatial and vertical distributions of κ_e could also be helpful for constraining estimates from other measurement procedures, e.g., chemical tracer [*Payn et al*., 2008] or geophysical techniques [*Ward et al*., 2012]. Knowledge of the actual flow velocities in parallel with pressure head information would, for example, substantially reduce uncertainties in hydraulic conductivity estimates. The added functionality of stream temperature time series should advance their role as an essential method within the array of techniques to characterize and monitor spatiotemporal variability in the hyporheic environment.

[73] **Acknowledgments.** We would like to thank Carolyn Bohn for assistance installing the wells and Jim McKean for providing materials and time for the initial measurements and background information for the interesting Bear Valley Creek experimental reach. We also thank Steve Wondzell and three anonymous reviewers for their insights and suggestions. Funding was provided for Frank Gariglio by the U.S. Forest Service, Department of Agriculture, RJVA 10-JV-11221634-247.

References

Anderson, M. P. (2005), Heat as a ground water tracer, *Ground Water*, *43*(6), 951–968.

Anderson, J. K., S. M. Wondzell, M. N. Gooseff, and R. Haggerty (2005), Patterns in stream longitudinal profiles and implications for hyporheic exchange flow at the H.J. Andrews Experimental Forest, Oregon, USA, *Hydrol. Process.*, *19*, 2931–2949.

Arras, K. O. (1998), An introduction to error propagation: Derivation, meaning and examples of equation *CY = FX CX FTX, Rep. EPFL-ASL-TR-98-01 R3*, Swiss Fed. Inst. of Technol. Lausanne (EPFL), Lausanne, Switzerland.

Arrigoni, A. S., G. C. Poole, L. A. K. Mertes, S. J. O'Daniel, W. W. Woessner, and S. A. Thomas (2008), Buffered, lagged, or cooled? Disentangling hyporheic influences on temperature cycles in stream channels, *Water Resour. Res.*, *44*, W09418, doi:10.1029/2007WR006480.

Baxter, C. V., and R. F. Hauer (2000), Geomorphology, hyporheic exchange, and selection of spawning habitat by bull trout (*Salvelinus confluentus*), *Can. J. Fish. Aquat. Sci.*, *57*, 1470–1481.

Bencala, K. E., M. N. Gooseff, and B. A. Kimball (2011), Rethinking hyporheic flow and transient storage to advance understanding of stream-catchment connections, *Water Resour. Res.*, *47*, W00H03, doi:10.1029/2010WR010066.

Boano, F., A. Demaria, R. Revelli, and L. Ridolfi (2010), Biogeochemical zonation due to intrameander hyporheic flow, *Water Resour. Res.*, *46*, W02511, doi:10.1029/2008WR007583.

Briggs, M. A., L. K. Lautz, J. M. McKenzie, R. P. Gordon, and D. K. Hare (2012), Using high-resolution distributed temperature sensing to quantify spatial and temporal variability in vertical hyporheic flux, *Water Resour. Res.*, *48*, W02527, doi:10.1029/2011WR011227.

Buffington, J. M., and D. Tonina (2009), Hyporheic exchange in mountain rivers. II: Effects of channel morphology on mechanics, scales, and rates of exchange, *Geogr. Compass*, *3*(3), 1038–1062.

Carslaw, H. S., and J. C. Jaeger (1959), *Conduction of Heat in Solids*, 510 pp., Clarendon, Oxford, U. K.

Clayton, J. L., J. King, and R. F. Thurow (1996), Evaluation of an ion adsorption method to estimate intragravel flow velocity in salmonid spawning gravel, *North Am. J. Fish. Manage.*, *16*, 167–174.

Constantz, J. (2008), Heat as a tracer to determine streambed water exchanges, *Water Resour. Res.*, *44*, W00D10, doi:10.1029/2008WR006996.

Constantz, J., and D. A. Stonestorm (2003), Heat as a tracer of water movement near streams, in *Heat as a Tool for Studying the Movement of Ground Water Near Streams*, edited by D. A. Stonestorm and J. Constantz, U. S. Geol. Surv., Denver, Colo.

Constantz, J., and C. L. Thomas (1996), The use of streambed temperature profiles to estimate the depth, duration, and rate of percolation beneath arroyos, *Water Resour. Res.*, *32*(12), 3597–3602.

Constantz, J., and C. L. Thomas (1997), Stream bed temperature profiles as indicators of percolation characteristics beneath arroyos in the middle Rio Grande basin, USA, *Hydrol. Process.*, *11*, 1621–1634.

Constantz, J., C. L. Thomas, and G. Zellweger (1994), Influence of diurnal variations in stream temperature on streamflow loss and groundwater recharge, *Water Resour. Res.*, *30*(12), 3253–3264.

Edwards, R. T. (1998), The hyporheic zone, in *River Ecology and Management: Lessons from the Pacific Coastal Ecoregion*, edited by R. J. Naiman and R. E. Bilby, pp. 399–429, Springer, New York.

Elliott, A., and N. H. Brooks (1997), Transfer of nonsorbing solutes to a streambed with bed forms: theory, *Water Resour. Res.*, *33*(1), 123–136.

Gariglio, F. P. (2012), Quantifying one-dimensional streambed seepage fluxes using thermal time series: Method development and application, Masters thesis, 82 pp., Univ. of Idaho, Boise, Idaho.

Geist, D. R. (2000), Hyporheic discharge of river water into fall chinook salmon (*Oncorhynchis tshawytscha*) spawning areas in the Hanford Reach, Columbia River, *Can. J. Fish. Aquat. Sci.*, *57*, 1647–1656.

Gordon, R. P., L. K. Lautz, M. A. Briggs, and J. M. McKenzie (2012), Automated calculation of vertical pore-water flux from field temperature time series using the VFLUX method and computer program, *J. Hydrol.*, *420–421*, 142–158, doi:10.1016/j.jhydrol.2011.11.053.

Goto, S., M. Yamano, and M. Kinoshita (2005), Thermal response of sediment with vertical fluid flow to periodic temperature variation at the surface, *J. Geophys. Res.*, *110*, B01106, doi:10.1029/2004JB003419.

Hatch, C., A. T. Fisher, J. S. Revenaugh, J. Constantz, and C. Ruehl (2006), Quantifying surface water-groundwater interactions using time series analysis of streambed thermal records: method development, *Water Resour. Res.*, *42*, W10410, doi:10.1029/2005WR004787.

ISO/IEC Guide 98-3 (2008), Uncertainty of measurement—part 3 guide to expression of uncertainty in measurement, Rep. GUM:1995, ISO, Geneva.

Jencso, K. G., B. L. McGlynn, M. N. Gooseff, S. M. Wondzell, K. E. Bencala, and L. A. Marshall (2009), Hydrologic connectivity between landscapes and streams: Transferring reach- and plot-scale understanding to the catchment scale, *Water Resour. Res.*, *45*, W04428, doi:10.1029/2008WR007225.

Kasahara, T., and A. R. Hill (2006), Hyporheic exchange flows induced by constructed riffles and steps in lowland streams in southern Ontario, Canada, *Hydrol. Process.*, *20*, 4287–4305.

Keery, J., A. Binley, N. Crook, and J. W. N. Smith (2007), Temporal and spatial variability of groundwater–surface water fluxes: Development and application of an analytical method using temperature time series, *J. Hydrol.*, *336*, 1–16.

Ku, H. H. (1966), Notes on the use of propagation of error formulas, *J. Res. Natl. Bur. Stand. C Eng. Instrum.*, *70*(4), 263–273.

Lautz, L. K. (2010), Impacts of nonideal field conditions on vertical water velocity estimates from streambed temperature time series, *Water Resour. Res.*, *46*, W01509, doi:10.1029/2009WR007917.

Lautz, L. K. (2012), Observing temporal patterns of vertical flux through streambed sediments using time-series analysis of temperature records, *J. Hydrol.*, *464–465*, 199–215, doi:10.1016/j.jhydrol.2012.07.006.

Lautz, L. K., and R. Ribaudo (2012), Scaling up point-in-space heat tracing of seepage flux using bed temperatures as a quantitative proxy, *Hydrogeol. J.*, *20*, 1223–1238, doi:10.1007/s10040-012-0870-2.

Lee, D. R., and J. A. Cherry (1978), A field exercise on groundwater flow using seepage meters and mini-piezometers, *J. Geol. Educ.*, *27*, 6–10.

Luce, C. H., and D. G. Tarboton (2010), Evaluation of alternative formulae for calculation of surface temperature in snowmelt models using frequency analysis of temperature observations, *Hydrol. Earth Syst. Sci.*, *14*, 535–543, doi:10.5194/hess-14-535-2010.

Marzadri, A., D. Tonina, A. Bellin, G. Vignoli, and M. Tubino (2010), Effects of bar topography on hyporheic flow in gravel-bed rivers, *Water Resour. Res.*, *46*, W07531, doi:10.1029/2009WR008285.

Marzadri, A., D. Tonina, and A. Bellin (2011), A semianalytical three-dimensional process-based model for hyporheic nitrogen dynamics in gravel bed rivers, *Water Resour. Res.*, *46*, W11518, doi:10.1029/2011WR010583.

Marzadri, A., D. Tonina, and A. Bellin (2012), Morphodynamic controls on redox conditions and on nitrogen dynamics within the hyporheic zone: Application to gravel bed rivers with alternate-bar morphology, *J. Geophys. Res.*, *117*, G00N10, doi:10.1029/2012JG001966.

Moore, R. D., P. Sutherland, T. Gomi, and A. Dhakal (2005), Thermal regime of a headwater stream within a clear-cut, coastal British Columbia, Canada, *Hydrol. Process.*, *19*, 2591–2608.

Orghidan, T. (1959), Ein neuer lebensraum des unterirdischen wassers: Der hyporheische biotop, *Arch. Hydrobiol.*, *55*, 392–414.

Payn, R. A., M. N. Gooseff, D. A. Benson, O. A. Cirpka, J. P. Zarnetske, W. B. Bowden, J. P. McNamara, and J. H. Bradford (2008), Comparison of instantaneous and constant-rate stream tracer experiments through non-parametric analysis of residence time distributions, *Water Resour. Res.*, *44*, W06404, doi:10.1029/2007WR006274.

Ren, J., and A. I. Packman (2004), Coupled stream-subsurface exchange of colloidal hematite and dissolved zinc, copper and phosphate, *Environ. Sci. Technol.*, *39*(17), 6387–6394.

Ren, J., and A. I. Packman (2007), Changes in fine sediment size distributions due to interactions with streambed sediments, *Sediment. Geol.*, *202*, 529–537, doi:10.1016/j.sedgeo.2007.03.021.

Salehin, M., A. I. Packman, and M. Paradis (2004), Hyporheic exchange with heterogeneous streambeds: laboratory experiments and modeling, *Water Resour. Res.*, *40*, W11504, doi:10.1029/2003WR002567.

Saltelli, A., S. Tarantola, F. Campolongo, and M. Ratto (2004), *Sensitivity Analysis in Practice: A Guide to Assessing Scientific Models*, John Wiley, Chichester.

Savant, A. S., D. D. Reible, and L. J. Thibodeaux (1987), Convective transport within stable river sediments, *Water Resour. Res.*, *23*(9), 1763–1768.

Schmidt, C., M. Martienssen, and E. Kalbus (2011), Influence of water flux and redox conditions on chlorobenzene concentrations in a contaminated streambed, *Hydrol. Process.*, *25*, 234–245, doi:10.1002/hyp.7839.

Selker, J., N. v. d. Giesen, M. Westhoff, W. Luxemburg, and M. B. Parlange (2006), Fiber optics opens window on stream dynamics, *Geophys. Res. Lett.*, *33*, L24401, doi:10.1029/2006GL027979.

Shanafield, M., C. Hatch, and G. Pohll (2011), Uncertainty in thermal time series analysis estimates of streambed water flux, *Water Resour. Res.*, *47*, W03504, doi:10.1029/2010WR009574.

Shope, C. L., J. E. Constantz, C. A. Cooper, D. M. Reeves, G. Pohll, and W. A. McKay (2012), Influence of a large fluvial island, streambed, and stream bank on surface water-groundwater fluxes and water table dynamics, *Water Resour. Res.*, *48*, W06512, doi:10.1029/2011WR011564.

Stallman, R. W. (1965), Steady one-dimensional fluid flow in a semi-infinite porous medium with sinusoidal surface temperature, *J. Geophys. Res.*, *70*(12), 2821–2827.

Stanford, J. A. (2006), Landscapes and riverscapes, in *Methods in Stream Ecology*, edited by F. R. Hauer and G. A. Lamberti, pp. 3–21, Academic, San Diego.

Stanford, J. A., and J. V. Ward (1988), The hyporheic habitat of river ecosystems, *Nature*, *335*, 64–65.

Stanford, J. A., and J. V. Ward (1993), An ecosystem perspective of alluvial rivers: connectivity and the hyporheic corridor, *J. North Am. Benthol. Soc.*, *12*(1), 48–60.

Suzuki, S. (1960), Percolation measurements based on heat flow through soil with special reference to paddy fields, *J. Geophys. Res.*, *65*(9), 2883–2885.

Taylor, C. J., D. J. Pedregal, P. C. Young, and W. Tych (2007), Environmental time series analysis and forecasting with the Captain toolbox, *Environ. Model. Software*, *22*, 797–814.

Terhune, L. D. B. (1958), The Mark VI Groundwater standpipe for measuring seepage through salmon spawning gravel, *J. Fish. Res. Board Can.*, *15*(5), 1027–1063.

Tonina, D., and J. M. Buffington (2007), Hyporheic exchange in gravel-bed rivers with pool-riffle morphology: laboratory experiments and three-dimensional modeling, *Water Resour. Res.*, *43*, W01421, doi:10.1029/2005WR004328.

Tonina, D., and J. M. Buffington (2009a), Hyporheic exchange in mountain rivers. I: Mechanics and environmental effects, *Geogr. Compass*, *3*(3), 1063–1086.

Tonina, D., and J. M. Buffington (2009b), A three-dimensional model for analyzing the effects of salmon redds on hyporheic exchange and egg pocket habitat, *Can. J. Fish. Aquat. Sci.*, *66*, 2157–2173.

Tonina, D., and J. M. Buffington (2011), Effects of stream discharge, alluvial depth and bar amplitude on hyporheic flow in pool-riffle channels, *Water Resour. Res.*, *47*, W08508, doi:10.1029/2010WR009140.

Triska, F. J., J. H. Duff, and R. J. Avanzino (1993), The role of water exchange between a stream channel and its hyporheic zone in nitrogen cycling at the terrestrial-aquatic interface, *Hydrobiologia*, *251*, 167–184.

Valett, M. H., S. G. Fisher, N. B. Grimm, and P. Camill (1994), Vertical hydrologic exchange and ecologic stability of a desert stream ecosystem, *Ecology*, *75*, 548–560.

Vogt, T., P. Schneider, L. Hahn-Woernle, and O. A. Cirpka (2010), Estimation of seepage rates in a losing stream by means of fiber-optic high-resolution vertical temperature profiling, *J. Hydrol.*, *380*, 154–164.

Ward, A. S., M. Fitzgerald, M. N. Gooseff, T. J. Voltz, A. M. Binley, and K. Singha (2012), Hydrologic and geomorphic controls on hyporheic exchange during base flow recession in a headwater mountain stream, *Water Resour. Res.*, *48*, W04513, doi:10.1029/2011WR011461.

Westhoff, M. C., M. N. Gooseff, T. A. Bogaard, and H. H. G. Savenije (2011), Quantifying hyporheic exchange at high spatial resolution using natural temperature variations along a first-order stream, *Water Resour. Res.*, *47*, W10508, doi:10.1029/2010WR009767.

Wondzell, S. M. (2011), The role of the hyporheic zone across stream networks, *Hydrol. Process.*, *25*, 3525–3532, doi:10.1002/hyp.8119.

Wroblicky, G. J., M. E. Campana, H. M. Valett, and C. N. Dahm (1998), Seasonal variation in surface-subsurface water exchange and lateral hyporheic area of two stream-aquifer systems, *Water Resour. Res.*, *34*(3), 317–328.

Zarnetske, J. P., M. N. Gooseff, B. W. Bowden, M. J. Greenwald, T. R. Brosten, J. H. Bradford, and J. P. McNamara (2008), Influence of morphology and permafrost dynamics on hyporheic exchange in arctic headwater streams under warming climate conditions, *Geophys. Res. Lett.*, *35*, L02501, doi:10.1029/2007GL032049.